

The impact of dissolved organic carbon and bacterial respiration on pCO₂ in experimental sea ice

Zhou, Jiayun; Kotovitch, Marie; Kaartokallio, Hermann; Moreau, Sebastien; Tison, Jean-Louis; Kattner, Gerhard; Dieckmann, Gerhard S.; Thomas, David N.; Delille, Bruno

Progress in Oceanography

DOI:

[10.1016/j.pocean.2015.12.005](https://doi.org/10.1016/j.pocean.2015.12.005)

Published: 01/02/2016

Peer reviewed version

[Cyswllt i'r cyhoeddiad / Link to publication](#)

Dyfyniad o'r fersiwn a gyhoeddwyd / Citation for published version (APA):

Zhou, J., Kotovitch, M., Kaartokallio, H., Moreau, S., Tison, J.-L., Kattner, G., Dieckmann, G. S., Thomas, D. N., & Delille, B. (2016). The impact of dissolved organic carbon and bacterial respiration on pCO₂ in experimental sea ice. *Progress in Oceanography*, 141, 153-167. <https://doi.org/10.1016/j.pocean.2015.12.005>

Hawliau Cyffredinol / General rights

Copyright and moral rights for the publications made accessible in the public portal are retained by the authors and/or other copyright owners and it is a condition of accessing publications that users recognise and abide by the legal requirements associated with these rights.

- Users may download and print one copy of any publication from the public portal for the purpose of private study or research.
- You may not further distribute the material or use it for any profit-making activity or commercial gain
- You may freely distribute the URL identifying the publication in the public portal ?

Take down policy

If you believe that this document breaches copyright please contact us providing details, and we will remove access to the work immediately and investigate your claim.

The impact of dissolved organic carbon and bacterial respiration on pCO₂ in experimental sea ice

Zhou, J.^{1,2,3}, M. Kotovitch^{1,2}, H. Kaartokallio⁴, S. Moreau⁵, J.-L. Tison¹, G. Kattner⁶, G. Dieckmann⁶, D.N. Thomas^{4, 7}, B. Delille²

¹ Laboratoire de glaciologie, DSTE, Université Libre de Bruxelles, Belgium

² Unité d'océanographie chimique, MARE, Université de Liège, Belgium

³ Division of Earth and Ocean Sciences, Duke University, Durham, NC, USA

⁴ Marine Research Centre, Finnish Environment Institute (SYKE), Helsinki, Finland

⁵ Georges Lemaître Centre for Earth and Climate Research, Earth and Life Institute, Université catholique de Louvain, Louvain-la-Neuve, Belgium

⁶ Alfred Wegener Institute Helmholtz Center for Polar and Marine Research, Bremerhaven, Germany

⁷ School of Ocean Sciences, Bangor University, Menai Bridge, United Kingdom

Abstract

Previous observations have shown that the partial pressure of carbon dioxide (pCO₂) in sea ice brines is generally higher in Arctic sea ice compared to those from the Antarctic sea ice, especially in winter and early spring. We hypothesized that these differences result from the higher dissolved organic carbon (DOC) content in Arctic seawater: Higher concentrations of DOC in seawater would be reflected in a greater DOC incorporation into sea ice, enhancing bacterial respiration, which in turn would increase the pCO₂ in the ice. To verify this hypothesis, we performed an experiment using two series of mesocosms: one was filled with seawater (SW) and the other one with seawater with an addition of filtered humic-rich river water (SWR). The addition of river water increased the DOC concentration of the water from a median of 142 μmol L⁻¹ in SW to 249 μmol L⁻¹ in SWR. Sea ice was grown in these mesocosms under the same physical conditions over 19 days. Microalgae and protists were absent, and only bacterial activity has been detected. We measured the DOC concentration, bacterial respiration, total alkalinity and pCO₂ in sea ice and the underlying seawater, and we calculated the changes in dissolved inorganic carbon (DIC) in both media. We found that bacterial respiration in ice was

higher in SWR: median bacterial respiration was 25 nmol C L⁻¹ h⁻¹ compared to 10 nmol C L⁻¹ h⁻¹ in SW. pCO₂ in ice was also higher in SWR with a median of 430 ppm compared to 356 ppm in SW. However, the differences in pCO₂ were larger within the ice interiors than at the surfaces or the bottom layers of the ice, where exchanges at the air-ice and ice-water interfaces might have reduced the differences. In addition, we used a model to simulate the differences of pCO₂ and DIC based on bacterial respiration. The model simulations support the experimental findings and further suggest that bacterial growth efficiency in the ice might be 0.15-0.2. It is thus credible that the higher pCO₂ in Arctic sea ice brines compared with those from the Antarctic sea ice were due to an elevated bacterial respiration, sustained by higher riverine DOC loads. These conclusions should hold for locations and time frames when bacterial activity is relatively dominant compared to algal activity, considering our experimental conditions.

Highlights (85 characters per highlight)

- Brine concentration/dilution causes the largest temporal changes of pCO₂ in ice
- Elevated BR due to riverine DOC addition increases pCO₂ in sea ice
- Gas exchange and the buffer effect further affect the bacterial impact on pCO₂

Keywords (up to six)

Sea ice, dissolved organic matter, carbon dioxide, bacterial activity, gas exchange

1. Introduction

Sea ice is formed from the freezing of seawater and covers about 6 % of the Earth's ocean surface. It has a heterogeneous structure composed of a matrix of pure ice and brine inclusions. Although sea ice is currently assumed to be impermeable to gas exchange in large-scale climate models, theoretical considerations (Golden et al., 1998) and pioneer gas measurements (Gosink et al., 1976) indicate that sea ice may be permeable under specific conditions of ice temperature and salinity. Measurements of pCO₂ in sea ice and brines have been intensified in both the Arctic (Crabeck et al., 2014; Geilfus et al., 2012a; Miller et al., 2011a, 2011b) and the Southern Ocean (Delille, 2006; Delille et al., 2007; Geilfus et al., 2014). The motivation for these measurements is to better understand the role of sea ice in the carbon cycle, including its role

in air-sea exchange of CO₂, and the potential feedback effects between the changing ice cover, CO₂ fluxes, and climate change.

Current measurements indicate that sea ice may act as a source or a sink for atmospheric CO₂, depending on the interplay of four processes:

(i) Brine concentration and dilution are associated with changes in ice temperature. When cooling a sea ice sample, some of the liquid water of the brine freezes, reducing the brine volume and inclusions and increasing the concentration of the impurities in the brine – this is the so-called brine concentration. In contrast, when warming a sea ice sample, some of the pure ice melts, increasing the volume of the brine inclusion and decreasing the concentration of the impurities in brine – this is the so-called brine dilution (Hunke et al., 2011; Notz and Worster, 2009).

(ii) Biological activity, which includes the photosynthesis and respiration by organisms, respectively, consumes and produces CO₂ (e.g., Papadimitriou et al., 2007).

(iii) The precipitation and dilution of calcium carbonate, which produces and consumes CO₂, respectively (Dieckmann et al., 2010, 2008; Geilfus et al., 2013), effectively alters the CO₂ budget in the ice when sea ice is semi-permeable, and when the calcium carbonate precipitates remain in the ice while the generated CO₂ is rejected into the under-ice water (Delille et al., 2014; Rysgaard et al., 2007) or to the atmosphere (Geilfus et al., 2013; Loose et al., 2011).

(iv) Gas transport through sea ice is not yet well constrained, but it is commonly assumed that sea ice is permeable for gas transport when its brine volume fraction is above 5 % (Golden et al., 1998). Brine drainage – the intensity of which is estimated using Raleigh numbers – is thought to be a significant process for ice-water exchange (Notz and Worster, 2009), while gas bubble formation potentially plays an important role in air-ice exchange (Moreau et al., 2014; Zhou et al., 2013). The diffusion of CO₂ through sea ice also affects air-ice exchange, but seems to be much slower, i.e., less efficient than gas bubble transport (Kotovitch et al., submitted; Loose et al., 2014).

Previous studies indicate that, for a given brine temperature, the pCO₂ in sea ice brine in the Arctic Ocean (Geilfus et al., 2014, 2012a) was generally higher than that in the Southern Ocean (Delille et al., 2014; Geilfus et al., 2014), especially when the average ice temperature was below -4°C – which generally corresponds to the winter and early spring period (Figure 1). In this study, we hypothesized that the higher pCO₂ was associated to the more intense bacterial respiration in the Arctic sea ice, due to the large input of riverine particulate organic carbon

(POC) and dissolved organic carbon (DOC) in the Arctic Ocean (e.g., Dittmar and Kattner (2003); Hansell et al. (2009)). Ice temperature is unlikely to explain the Arctic-Antarctic discrepancies, because at a given temperature, the effect of brine concentration on $p\text{CO}_2$ is expected to be the same in both hemispheres. However, the impact of DOC availability on bacterial respiration and $p\text{CO}_2$ in sea ice has not yet been demonstrated by systematic DOC and POC measurements in parallel. Therefore we performed an indoor experiment using two series of mesocosms: One was filled with seawater (SW) and another with seawater and an addition of filtered river water (SWR) to simulate riverine DOC input. The objective of the present paper is to verify whether or not higher DOC concentrations in seawater, due to an addition of riverine DOC, induce larger DOC concentrations in sea ice, which in turn enhance bacterial respiration and $p\text{CO}_2$ in the ice.

2. Material and methods

2.1 Experimental setting, and sampling routine and initial conditions

The experimental setting and sampling routine has been described in Zhou et al. (2014). Briefly, we ran a 19-day experiment in the Arctic Environmental Test Basin facility of the Hamburg Ship Model Basin (www.hsva.de) from May to June 2012. We used 21 polyethylene experimental mesocosms each with a volume of 1.2 m³. Eleven of the mesocosms were filled with 1000 L of seawater from the North Sea (referred here after as SW), and the remaining ten were filled with 900 L of seawater from the North Sea and 100 L of filtered river water collected at a peat-dominated catchment of the River Kiiminkijoki, in Finland (referred here after as SWR).

The addition of river water caused a significantly higher DOC concentration in the SWR mesocosms (paired t-test, $p < 0.001$): Median salinity-normalized DOC concentrations were 140 $\mu\text{mol L}^{-1}$ in SW and 251 $\mu\text{mol L}^{-1}$ in SWR (salinity 30.9), with a standard deviation of 3 % in the SW mesocosms and 9 % in SWR. However, salinity-normalized dissolved organic nitrogen (DON) was not significantly different between both mesocosm series (median of 16 $\mu\text{mol L}^{-1}$ in SW and 19 $\mu\text{mol L}^{-1}$ in SWR), because its concentration in river and North Sea water were almost the same, and the standard deviation was relatively high (17 %) in both SW and SWR mesocosms. The carbonate chemistry was also not significantly different for both mesocosm series: median salinity-normalized total alkalinity was 2314 $\mu\text{mol kg}^{-1}$ in SW and 2336 $\mu\text{mol kg}^{-1}$ in SWR; median salinity-normalized dissolved inorganic carbon (DIC) were 2113 $\mu\text{mol kg}^{-1}$ in SW and 2161 $\mu\text{mol kg}^{-1}$ in SWR; and median $p\text{CO}_2$ were 212 ppm in SW and 231

ppm in SWR, respectively. The salinities of the SWR mesocosms were adjusted to the SW values by adding aquarium standard salt (Tropic Marin[®]). Nitrate (NO₃⁻) and phosphate (PO₄³⁻) concentrations were also adjusted to concentrations that would not limit bacterial growth in both series of mesocosms, and that were representative of areas in both Arctic and Southern Oceans (Zhou et al., 2014).

Ice was grown from day 0 to 14, during which the air temperature was maintained at -14 °C, and then the air temperature was increased to -1 °C to trigger a decay phase. We collected ice, brine and seawater at various occasions from day 0 to day 19 for the measurements of temperature, salinity, DOC, inorganic nutrients, bacterial abundance, and bacterial activity (Zhou et al., 2014), as well as pCO₂ and total alkalinity.

Because the physical constraints were similar for both the SW and SWR mesocosms, we expected bacterial activity to be the only process affecting the difference of pCO₂ in both water and ice. Median bacterial abundance was 922 cells L⁻¹ in SW at the beginning of the experiment and was not significantly different from the 972 cells L⁻¹ in SWR. Protists and active photoautotrophs were absent in the experiment (checked by microscopy and epifluorescence microscopy, respectively). As a corollary, there was no autochthonous production of DOC and our experiment focuses on the impact of the additional allochthonous DOC (added by the river water) on bacterial respiration and pCO₂ in both water and ice. Although photoautotrophs were absent in our experiments, we believe that it would not drastically affect the verification of the hypothesis, because the largest observed difference of pCO₂ in brine corresponds to the lowest ice temperature (Figure 1), which mostly correspond to the ice interior (over winter and early spring) where algal activity is relatively limited compared to the bacterial activity (Baer et al., 2015).

2.2 Brine volume fraction and Raleigh number

The brine volume fraction is used here as a proxy of sea ice permeability and is calculated from the ice temperature and salinity following the relationship of Cox and Weeks (1983). We assume that the sea ice was permeable for a brine volume fraction exceeding 5 % (Golden et al., 1998). We also calculated the Rayleigh number (Ra), which is a proxy for brine convection as described by Notz and Worster (2008). Theoretically, convection is possible in an ice layer (of a thickness h) when Ra exceeds 1 and decreases from the top to the bottom of that layer (Notz, personal communication). We thus simply assume the critical Ra being 1 following those theoretical considerations.

2.3 DOC and DON

Samples for the determination of dissolved organic carbon (DOC) and total dissolved nitrogen (TDN) were stored frozen (-20 °C) in glass vials (Wheaton; pre-combusted at 500 °C for 5 h) and determined by high temperature catalytic oxidation and subsequent non-dispersive infrared spectroscopy and chemiluminescence detection, respectively (TOC-VCPN, Shimadzu). After each batch of five samples, one reference standard (DOC-DSR, Hansell Research Lab, University of Miami, US), one ultrapure-water blank and one potassium hydrogen phthalate standard for DOC and potassium nitrate for TDN were measured. DON concentrations were calculated as difference of TDN and inorganic nitrogen. The accuracy of the measurements was $\pm 5 \%$.

2.4 Bacterial respiration

Bacterial respiration has been calculated as the difference between the bacterial carbon demand and bacterial production. We measured bacterial production (see below) and assumed that it represented 34.8 % (bacterial growth efficiency, BGE) of the bacterial carbon demand to deduce the bacterial respiration. BGE was derived as mean estimate from available sources for sea-ice bacteria or bacteria in very cold temperatures (Kuparinen et al., 2011; Nguyen and Maranger, 2011; Rivkin and Legendre, 2001).

For the bacterial production measurements, samples containing a known amount of crushed ice and sterile-filtered seawater (Kaartokallio, 2004) were prepared in a cold room as follows: each intact 5–10 cm ice core section was crushed using a spike and electrical ice cube crusher. Approximately 10 mL of crushed ice was weighed in a scintillation vial. To better simulate the brine pocket salinity and ensure an even distribution of labelled substrate, 3 ± 1 mL of sterile filtered (through a 0.2 μm filter) seawater from the sample bags were added to the scintillation vials. Bacterial production was measured immediately after sample collection using the [^3H]-thymidine incorporation method (Fuhrman and Azam, 1982, 1980). Two aliquots and a formaldehyde-fixed absorption blank were amended with [^3H]-thymidine (PerkinElmer, USA, specific activity 20 Ci mmol $^{-1}$). The added concentration was 30 nmol L $^{-1}$ for all sample types. The samples were incubated in the dark at -0.6 °C on crushed ice in an insulated container according to the projected level of activity: ice samples were incubated between 19 h and 22 h, water and brine samples between 4 h and 6 h. The incubations were stopped by addition of formaldehyde and samples were processed using the standard cold-TCA extraction and filtration procedure. Samples were extracted for 15 minutes in ice-cold 5 % TCA and labelled macromolecules collected on 0.2 μm mixed cellulose ester membrane filters (Osmonics). Filters

were rinsed five times with ice-cold 5% TCA and placed in clean scintillation vials. A Wallac WinSpectral 1414 counter and InstaGel (Perkin-Elmer) cocktail were used in scintillation counting. Bacterial production was calculated using a cell conversion factor of 2.09×10^{18} cells mol^{-1} (Smith and Clement, 1990), a cell volume of $0.3 \mu\text{m}^3$ (Kaartokallio, 2004; Smith and Clement, 1990) and a carbon conversion factor of $0.12 \text{ pgC } \mu\text{m}^{-3}$ (Nagata and Watanabe, 1990; Pelegrí et al., 1999).

2.5 pCO₂

The pCO₂ of the seawater was measured *in-situ* using a custom-made equilibration system, which is described in Delille et al. (2014). Briefly, the system consists of a membrane contractor equilibrator (Membrana[®], Liqui-cell) that is connected to a non-dispersive infrared gas analyser (IRGA, Li-Cor[®] 6262) via a closed air loop. Seawater and air flow rates through the equilibrator and IRGA were approximately 2 L min^{-1} and 3 L min^{-1} , respectively. Temperature was simultaneously measured *in situ* and at the outlet of the equilibrator using Li-Cor[®] temperature sensors. Temperature correction of pCO₂ was applied assuming that the relation of Copin-Montegut (1988) is valid at low temperature and high salinity. Data were stored on a Li-Cor[®] Li-1400 data logger. All devices, except the peristaltic pump, were enclosed in an insulated box that contained a 12 V power source providing enough warming to keep the inside temperature above 0°C . Uncertainty is less than $5 \mu\text{atm}$.

The method for the pCO₂ measurements in ice is the same as in Geilfus et al. (2012b), but with longer equilibrium times following Crabeck et al. (2014). The ice samples were cut with a band saw, in a cold room at -25°C and adjusted to the container's inner volume ($4 \text{ cm} \times 4 \text{ cm} \times 4.4 \text{ cm}$). The sample was sanded down using fine-grained sandpaper so that it fitted tightly into the container to minimise the headspace volume. Then, the container was placed into a Dewar vessel filled with ethanol, which was cooled to -30°C with liquid nitrogen. The container was then connected to the extraction line (tap closed). The line was first evacuated down to a pressure of 10^{-3} Torr, after which the container was evacuated for 5 min. The low temperature of the vessel insures sea ice impermeability, i.e., the CO₂ of the ice was not vacuumed during this process. The standard gas was then injected into the container at 1013 mbar. The container was subsequently removed from the extraction line (tap closed), placed in a thin plastic bag and submerged in a thermostatic bath (set to the *in situ* temperature, i.e., that was measured on the ice samples directly after the extraction). After 20 h of equilibrium, the container was placed in a Dewar filled with ethanol cooled at the *in situ* temperature and reconnected to the evacuated (10^{-3} Torr) extraction line. At the same time, a water trap consisting of a Dewar filled with an

ethanol bath at -65 °C was placed on the line just before the GC. The gas was finally injected into the GC. Immediately after the injection, the ice sample temperature was measured using a calibrated thermometer (Testo 720®). Reproducibility of the measurement is 2.9%.

2.6 TA and DIC

Total alkalinity (TA) was measured on melted bulk ice and seawater samples. Ice cores were cut at a 2 cm-depth resolution (about 50 g of ice for each section) and melted. Melted bulk ice and seawater samples were poisoned with a solution of supersaturated HgCl₂ and then stored in the dark, until analysis (one year after the sampling). TA was measured by open-cell titration with 0.11 M HCl and the endpoints were determined according to Gran (1952). Routine analyses of Certified Reference Materials (provided by A. G. Dickson, Scripps Institution of Oceanography) ensured that the uncertainty of the TA measurements was less than 4 µmol kg⁻¹.

Dissolved inorganic carbon (DIC) was calculated from TA and pCO₂ using CO2SYS (Lewis and Wallace, 1998), the CO₂ acidity constants of Mehrbach et al. (1973) refitted according to Dickson and Millero (1987) and other constants advocated by DOE (1994). We assumed that the CO₂ dissociation constants were applicable at sub-zero temperatures as suggested by Marion (2001) and Delille et al. (2007). To compare DIC in seawater and in melted bulk ice, we normalized the DIC values to a salinity of 7 (DIC₇), for consistency with previous studies. The salinity of 7 is also the mean salinity of the ice in this study. Uncertainty of DIC₇ deduced from the reproducibility of TA and pCO₂ has been evaluated to be 0.8 µmol kg⁻¹ using Monte Carlo procedure (Anderson, 1976).

2.7 Differences between the SW and SWR series and statistical tests

The ice thickness was different between the SW and SWR mesocosms (up to 3 cm (15 %) of difference) at day 14 and day 15. This was due to an unavoidable temperature gradient in the experimental basin (Zhou et al., 2014). In spite of the gradient of temperature in the experimental basin, we do not think that it has affected the results. The SW and SWR mesocosms sampled the same day were adjacent mesocosms located on the same row (minimizing the differences in physical conditions). For day-to-day sampling, the SW/SWR pairs of mesocosms were randomly selected in space. In spite of that random selection, we still could see a trend in the physical parameters (Zhou et al., 2014), which means that the temperature gradient in the experimental basin did not significantly bias our results. However, to be rigorous, when the ice thicknesses were different for SW and SWR, we calculated the difference of the parameters (e.g., pCO₂) on normalized ice depth, and then multiplied the

normalized ice depth by the ice thickness of the SW series. In addition, two parameters were assumed to be similar (i.e., no significant difference between the SW and SWR series), when a minimum similarity score of 0.95 was achieved.

3. Results

3.1 Physical sea ice conditions

As described in Zhou et al. (2014), the differences in the physical properties of the ice between the SW and SWR mesocosms were insignificant. The brine volume fraction was above 5 % during the whole experiment, which suggests that the ice was always permeable (Golden et al., 1998). The maxima in the brine volume fraction were all found at the bottom of the ice, while the minima were found in the ice interior, and decreased from 13.3 % on day 1 to 5.7 % on day 14, but increased from day 15 onwards, due to the increase of the air temperature from -14 °C to -1 °C. The Rayleigh numbers were higher than 1, indicating favourable conditions for brine convection at all ice depths on day 2, and thereafter only at the bottom of the ice until day 14. From day 15 onwards, the Rayleigh numbers were always below 1, indicating that brine convection was unlikely (Figure 2). A large difference of Ra has been observed at the bottom of the ice between SW and SWR mesocosms, from day 6 to 14, and was likely due to an underestimation of salinity in SWR, and the propagation of that bias in the calculation of Ra (Zhou et al., 2014), but is not significant for the purpose of the present study.

3.2 DOC and DON

DOC concentrations in sea ice and water and their difference between the SW and the SWR mesocosms have been presented and discussed in Zhou et al. (2014) and Jørgensen et al. (2015). Most importantly, the salinity-normalized DOC concentrations in the underlying water were higher in the SWR mesocosms than in the SW mesocosm during the experiment (paired t-test, $p < 0.001$); the medians were $142 \mu\text{mol L}^{-1}$ in SW and $246 \mu\text{mol L}^{-1}$ in SWR (salinity of 30.9), which were similar to the initial conditions. Median DOC concentrations in ice were $71 \mu\text{mol L}^{-1}$ in SW and $109 \mu\text{mol L}^{-1}$ in SWR. These are equivalent to $287 \mu\text{mol L}^{-1}$ and $409 \mu\text{mol L}^{-1}$ respectively, once normalized to a salinity of 30.9 as for the underlying water (paired t-test, $p < 0.001$); they are higher than the values in water, which indicate a preferential retention of DOC in sea ice.

DON concentrations have not been systematically measured as for DOC ($n=18$ in water and 15 in ice for DON compared to $n=20$ and 110, respectively, for DOC (SW+SWR)). The limited

number of data we have show that the salinity-normalized DON concentrations were not significantly different in SW and SWR mesocosms, not before the experiment (median of 21 $\mu\text{mol L}^{-1}$), or during the experiment, in both the water and ice (medians of 17 $\mu\text{mol L}^{-1}$ and 21 $\mu\text{mol L}^{-1}$, respectively) (data not shown). No significant trend in DON has been detected in the water and the ice over the experiment.

3.3 Bacterial activity

Median bacterial abundance in the underlying water increased over the experiment, reaching 1470 cells L^{-1} in SW and 1505 cells L^{-1} in SWR. This difference was not significant, despite the significantly higher bacterial production (BP) in the SWR mesocosms (paired t-test, $p=0.007$), with a median of 69 $\text{nmolC L}^{-1} \text{h}^{-1}$ in SWR compared to 51 $\text{nmolC L}^{-1} \text{h}^{-1}$ in SW. Bacterial respiration (BR) in water was also higher in the SWR mesocosms (paired t-test, $p=0.027$), with a median of 98 $\text{nmolC L}^{-1} \text{h}^{-1}$ in SW and 129 $\text{nmolC L}^{-1} \text{h}^{-1}$ in SWR, respectively (Figure 3a, left).

Median bacteria abundance in ice was 299 cells L^{-1} in SW and 352 cells L^{-1} in SWR, with a net loss of 24 cells $\text{L}^{-1} \text{d}^{-1}$ in SW and 16 cells $\text{L}^{-1} \text{d}^{-1}$ in SWR over the experiment. Median BP was 5 $\text{nmolC L}^{-1} \text{h}^{-1}$ in SW and 13 $\text{nmolC L}^{-1} \text{h}^{-1}$ in SWR, and median BR, 10 $\text{nmol L}^{-1} \text{h}^{-1}$ in SW and 25 $\text{nmol L}^{-1} \text{h}^{-1}$ in SWR (Fig. 3a, right). To compare bacterial activity in ice with that in seawater, we assumed that all these parameters were conservative against salinity. Once normalized to a salinity of 30.9, median bacterial abundance reached 1220 cells L^{-1} in SW and 1440 cells L^{-1} in SWR; median BP of 23 $\text{nmolC L}^{-1} \text{h}^{-1}$ in SW and 53 $\text{nmolC L}^{-1} \text{h}^{-1}$ in SWR; and median BR of 42 $\text{nmolC L}^{-1} \text{h}^{-1}$ in SW and 100 $\text{nmolC L}^{-1} \text{h}^{-1}$ in SWR. Note that all these values were higher in SWR than in SW (paired t-test, $p<0.001$), but lower than in seawater (paired t-test, $p<0.001$ for BP and BR in SWR; $p=0.001$ in SW; $p=0.004$ for bacterial abundance in SW but no significance has been found for bacterial abundance in SWR). The vertical distribution of BR in ice was similar in the SW and SWR mesocosms (Figure 4): It increased from the top to the bottom of the ice. The difference between both mesocosm series generally increased from the top to the bottom of the ice, where the largest differences were observed.

3.4 DIC₇

For data comparison with literature, we normalized DIC to a salinity of 7. Differences of DIC₇ between SW and SWR were not significant for both the under-ice water and the ice. DIC₇ in seawater varied around a median value of 455 $\mu\text{mol kg}^{-1}$, when excluding the outlier of SWR on day 5. Median DIC₇ in ice for the same mesocosms was slightly higher than in seawater,

reaching $486 \mu\text{mol kg}^{-1}$ (Figure 3). DIC_7 in both media increased from day 2 to day 16 and then remained constant. DIC_7 in the ice increased from the top to the bottom of the ice in SW and SWR mesocosms (Figure 5). At the bottom of the ice, it increased throughout the experiment and was always higher than the DIC_7 of the under-ice water by an average of $40 \mu\text{mol kg}^{-1}$. The difference of DIC_7 between SWR and SW was higher in the ice interior at 8 cm to 12 cm depth. For comparison with bacterial respiration in ice, median DIC in ice that is not salinity-normalized was $434 \mu\text{mol kg}^{-1}$, which is equivalent to $400 \mu\text{mol L}^{-1}$.

3.5 pCO_2

pCO_2 in water was not significantly different between both mesocosm series, with a median pCO_2 of 270 ppm. pCO_2 in ice was also not significantly different between both mesocosm series probably as a result of the large variability. Median pCO_2 in ice was 360 ppm with a large range spanning from 223 ppm to 651 ppm (Figure 3). Median pCO_2 was higher in the ice than in seawater during ice growth (day 2 to day 14), despite similar concentrations of DIC_7 in the seawater and in the ice and lower bacterial respiration in ice than in seawater (Figure 3c, sections 3.3 and 3.4).

The pCO_2 in ice had a similar temporal evolution in the SW and SWR mesocosms (Figures 3c and 6). Considering that the average atmospheric pCO_2 was 460 ppm during the experiment (Kotovitch et al. submitted), pCO_2 in ice was at first under-saturated on day 2, and then became increasingly supersaturated until day 14, and then under-saturated again from day 15 onwards. Despite the similar temporal evolution of pCO_2 in ice, pCO_2 was generally higher in the SWR mesocosms, with a median value of 430 ppm compared to the 356 ppm in the SW mesocosms. The differences in pCO_2 were generally higher from the top to the ice interior to about 8 cm depth, except on day 2, when the ice was relatively thin (6 cm); on days 5 and 19, the difference of pCO_2 at the bottom of the ice was likely biased due to the large difference of CO_2 in the under-ice water (Figure 3c, left). Indeed, for days 5 and 19, the differences in pCO_2 in the under-ice water between SW and SWR were 100 ppm and 86 ppm, respectively, while they generally approached 0 ppm to 20 ppm in the other mesocosms on all other sampling days (Figure 3c, left).

4. Discussion

The addition of river water led to an enrichment of the overall DOC concentrations in the SWR water, compared to SW, by a factor of 1.8 ($251 \mu\text{mol L}^{-1} / 140 \mu\text{mol L}^{-1}$). The preferential retention of DOC in sea ice during ice formation (Giannelli et al., 2001; Müller et al., 2013;

Zhou et al., 2014) led to a salinity-normalized DOC concentration in ice that was higher than the under-ice water ($409 \mu\text{mol L}^{-1} / 287 \mu\text{mol L}^{-1}$), but the difference of DOC enrichment between SWR and SW dropped to 1.4. The mechanisms underlying the preferential retention of DOC in sea ice is not fully understood, but other measurements during our experiment suggested that sea ice formation increases the lability of DOM in ice (Jørgensen et al., 2015). We therefore speculate that the more labile forms of DOM were better retained in sea ice than the more refractory ones. Because SWR contained a larger fraction of less labile terrestrial humic acids due to the addition of river water (Jørgensen et al., 2015), the DOC enrichment in ice in SWR was lower than in SW. We show below that the segregation of DOC between water and ice, in addition to the difference in temperature and salinity, likely contributed to the difference of bacterial activity in water and ice.

4.1 Impact of riverine DOC addition on bacterial activity

Available under-ice or partially ice covered water respiration estimates for Western Arctic vary from 19 to $39 \text{ nmol C L}^{-1} \text{ h}^{-1}$ (Kirchman et al., 2009; Nguyen and Maranger, 2011; Nguyen et al., 2012), which is an order of magnitude lower than our respiration estimate for water (median of $98 \text{ nmol C L}^{-1} \text{ h}^{-1}$ in SW and $129 \text{ nmol C L}^{-1} \text{ h}^{-1}$). However, our experimental system was based on North Sea water with a high DOC content and added inorganic nutrients, which are both likely to support higher bacterial production than the more oligotrophic Arctic waters.

Assuming that bacterial activity took place 24 hours a day, a consumption of $23.3 \mu\text{mol C L}^{-1}$ in SW and $31.5 \mu\text{mol C L}^{-1}$ in SWR is necessary to support the observed BP over the 19-day experiment. These represent 16 % and 13 % of the DOC pool, respectively. However, no significant changes have been detected in the DOC and DON concentrations in the under-ice water, or in the concentrations of inorganic nutrients (Zhou et al., 2014). A possible explanation is that bacteria used particulate organic matter (POM) as a carbon source for growth, despite the large pool of DOC. We did not measure POM concentrations in our experiment, but considering the absence of protists and active algae in seawater (in spite of the use of unfiltered seawater), we assumed that they died in the mesocosms, providing an additional source of carbon for bacterial growth. If this assumption is correct, BP would represent a smaller fraction of the DOC pool. The fraction was likely smaller than 3 % in SW and 9 % in SWR (the standard deviation of DOC concentrations among the mesocosms in the initial waters), because we would have detected significant changes otherwise.

Although BP only represented a small fraction of the DOC pool, the addition of riverine DOC was the most plausible factor causing the significantly higher BP in the SW water, since all the other parameters (bacterial abundance, DON, inorganic nutrients, temperature, and presumably POC) were not significantly different between the SW and SWR mesocosms.

Published sea-ice respiration values originate from batch culture incubations using sea ice bacteria and are either derived from total Arctic sea ice community respiration measurements made in water phase incubations (Nguyen and Maranger, 2011) or from experimental systems with Baltic sea ice bacteria (Kuparinen et al., 2011). The estimated mean bacterial respiration in western Arctic ice was $50 \text{ nmol C L}^{-1} \text{ h}^{-1}$ (Nguyen and Maranger, 2011) and in the Baltic Sea experiments approximately $80 \text{ nmol C L}^{-1} \text{ h}^{-1}$ (Kuparinen et al., 2011). Our respiration estimate for ice was lower but of the same order of magnitude, despite major differences in methodology and experimental setup.

Bacterial activity in ice was different from that in the under-ice water. Bacterial abundance in sea ice was lower than in seawater, even when normalized to the same salinity. This has been observed before in similar experiments (Eronen-Rasimus et al., 2014) and likely resulted from the low ice temperature and high brine salinity, which favour the selection of psychrotrophic and psychrophilic bacteria (Helmke and Weyland, 1995).

Although the overall BP and bacterial abundance were lower in the ice than in the under-ice water, the ratio between both the SW and SWR mesocosms were more pronounced in the ice. Bacterial production in SWR ice was 2.6 times higher than in SW, i.e., twice as high as the ratio (SWR/SW) observed in the water. Bacterial abundance was 20 % higher than the SW ice, while no significant difference was found in the under-ice water. The only plausible factor driving these SWR/SW differences in ice was the higher DOC concentration in the SWR ice. Ice microalgae and protists were indeed absent (verified by microscopy) and no significant difference has been found in the DON concentrations and the physical properties of the ice.

It is curious as to why the differences of BP between both series of mesocosms were larger in ice (SWR/SW ratio of 2.6) than in the water (ratio of 1.3), considering that the differences of DOC concentrations between both mesocosms series decreased (ratio of 1.4 in ice compared to 1.8 in water). This might be associated with the changes of the organic matter quality towards more labile (bioavailable) forms in the ice during sea ice formation (Jørgensen et al., 2015). In seawater, the addition of riverine DOC promoted higher BP in the SWR mesocosms. In sea ice, the absolute DOC concentrations in SWR are not only higher than in SW, their lability might also have increased compared to the SWR under-ice water; both might explain the larger

difference of BP in ice between the SW and SWR mesocosms compared to the under-ice water. DOC can directly contribute to bacterial growth as a carbon source; it may also support the formation of exopolymeric substances (EPS) in growing sea ice (Aslam et al., 2012) – a substance that is known to support microorganisms survival under the extreme conditions in sea ice (Krembs et al., 2011). Further, it might also have favoured the development of a bacterial community that is different from that in SW, as it has been observed by Eronen-Rasimus et al. (2014).

4.2 Similarities of DIC and pCO₂ in ice in the SW and SWR mesocosms

DIC₇, which ranged from 423 $\mu\text{mol kg}^{-1}$ to 512 $\mu\text{mol kg}^{-1}$ (in SW and SWR), was consistent with previous measurements on natural sea ice (Geilfus et al., 2014, 2012a; Rysgaard et al., 2007). pCO₂ measurements for natural sea ice are scarce (Crabeck et al., 2014; Geilfus et al., 2014) and have been mainly obtained from the spring-summer period. Therefore, they were generally under-saturated relative to the atmosphere (i.e., below 400 ppm) (Crabeck et al., 2014; Geilfus et al., 2014). The pCO₂ below 400 ppm in ice during the decay period of our experiment was thus consistent with data from natural sea ice in spring and summer. Because of the lack of pCO₂ measurements in natural ice during ice growth (and especially in autumn), we extended the comparison to the pCO₂ in brine. Considering that the median ice temperature approached -4.5 °C during ice growth in this experiment (Zhou et al., 2014), and that temperature would correspond to a pCO₂ of about 800 ppm in Arctic sea ice brine (Figure 1), our in situ measurements of up to 724 ppm are realistic.

Brine concentration and dilution and gas transport are likely to be the two main physical processes determining the similarities in the temporal and vertical pattern of pCO₂ between the SW and SWR mesocosms (Figure 7). When plotting pCO₂ in ice (SW and SWR) against the brine volume fraction, 10 mesocosms over 14 (represented by the circles on Figure 7) followed a decreasing trend ($r^2 = 0.836$, $p < 0.03$). These events include the very beginning of ice growth (day 2) and the ice growth and ice decay, except day 5, day 15 and two other outliers.

When cooling an ice sample, part of the water present in the brine inclusion will freeze, forming a thicker surrounding pure ice matrix, which results in a higher concentration of the dissolved constituents into smaller brine inclusions. Therefore, pCO₂ in sea ice became increasingly supersaturated, as the brine volume fraction decreased (from day 0 to day 14). In contrast, when warming an ice sample, the surrounding pure ice matrix is expected to melt, increasing the size of the brine inclusion and diluting the concentration of the dissolved constituents in the brines.

pCO₂ in sea ice thus became under-saturated as a result of the warming air temperature (from day 15 onwards) (Figures 6 and 7).

A rapid and one-time decrease of pCO₂ in ice was observed on day 15. This was a particular event, occurring the day after the rapid increase of the air temperature, when the sea ice surface temperature sharply increased from -10 °C to -2 °C within 20 hours (Kotovitch et al., submitted). Different processes may explain this drastic decrease of pCO₂, e.g., rapid release of gas bubbles (Zhou et al., 2013) and/or melt of CO₂-poor surface ice layers and seepage of the meltwater (Geilfus et al., 2014), while the equilibrium of air-ice pCO₂ occurs at a much slower rate. However, considering that day 15 was a particular event, it is unlikely that these pCO₂ changes would be representative of those observed in natural conditions, so we will not further discuss the different plausible processes. Another outlier corresponded to the surface ice layer, where ice melt might have induced the low pCO₂ (153 ppm). We currently have no explanation for the other outlier on day 5. Nevertheless, excluding these data, pCO₂ was significantly correlated with the brine volume fraction, which indicates the major role of brine concentration and dilution in regulating pCO₂ in ice.

To further demonstrate the importance of brine concentration and dilution for pCO₂ dynamics, we compared our values with the theoretical pCO₂ considering only the changes in temperature and brine salinity. The theoretical pCO₂ was calculated using the CO2SYS program (Lewis and Wallace, 1998), the constants of Goyet and Poisson (1989), and the median temperature, salinity, total alkalinity and DIC in the parent water as initial conditions. We then used the median ice salinity (6.3) to calculate the brine volume fraction associated with each prescribed temperature. The theoretical pCO₂ (red curve in Figure 7) reproduced the observations well between 10 % and 20 % of brine volume fraction (i.e., for about half of the data set), but overestimated the pCO₂ in ice (up to 320 ppm, i.e., 44 %) for brine volume fractions below 10 %. We attribute this overestimation to a significant escape of CO₂ from the ice to the atmosphere during ice growth, which is not taken into account by the CO2SYS. Another explanation could be that the constants used in CO2SYS might be incorrect for sea ice, since they were developed for temperature and salinity ranges of seawater, which are less extreme than those of sea ice. However, the error in the estimate of pCO₂ should approach 10 % according to Brown et al. (2014), when using TA and DIC as input parameters and the constants of Goyet and Poisson (1989). Hence, the error on the seawater-derived constant is not great enough to explain the difference in pCO₂ between the CO2SYS estimate and the observations,

and therefore the escape of CO₂ from the ice to the atmosphere remains the most plausible explanation.

The DIC₇ profiles confirm that gas transport through sea ice affected pCO₂ in ice (Figure 5), in addition to brine concentration and dilution. If sea ice would be a closed system, and the air-ice and ice-water exchange absent, DIC would be conservative against salinity. Hence, the value of DIC₇ would be the same at all ice depths and in seawater. In our study, the ice was always permeable, with the brine volume fraction always above 5 % (Golden et al., 1998). Gas exchange through the ice was thus possible and resulted in the deviation of the DIC₇ in ice from the conservative behaviour. Values of DIC₇ in ice that decreased from the bottom to the top of the ice indicate an escape of CO₂ from the surface of the ice to the atmosphere (Figure 5) (Geilfus et al., 2013), and the observed decrease was also consistent with the air-ice fluxes we have measured during the growth phase of this experiment (Kotovitch et al., submitted). At the bottom of the ice, DIC₇, which approached the values in the under-ice water, indicate that ice-water exchange took place, which was possible through brine convection (high Rayleigh number, Figure 2). The DIC₇ at the bottom of the ice increased throughout the entire period of ice growth, following the increase in DIC₇ in the under-ice water as a result of the expulsion of DIC from the ice and bacterial respiration in the water during ice growth (Figure 3) (Moreau et al., submitted).

4.3 Differences of DIC and pCO₂ in ice between the SW and SWR mesocosms

DIC₇ and pCO₂ in ice were higher in SWR than in SW. However, these differences between SW and SWR were not significant, despite the significantly higher BR in SWR, which should result in a larger accumulation of DIC and CO₂ in SWR. Because the dynamics of DIC₇ and pCO₂ not only depend on bacterial activity, but also on physical processes (which were the same in both SW and SWR), the absence of significant differences might indicate that the physical processes have offset the bacterial impact on DIC₇ and pCO₂. For instance, if the differences of DIC₇ and pCO₂ were only due to bacterial activity, it is curious as to why the largest differences of DIC₇ and pCO₂ were observed in the ice interior (Figures 5 and 6), instead of at the bottom of the ice, where the difference in bacterial respiration was the largest. We interpret this as the result of gas exchange at the air-ice and ice-water interfaces, in addition to bacterial respiration. Since the difference of pCO₂ was smaller between the bottom of the ice and the water than between the surface of the ice and the atmosphere, we conclude that ice-water exchange might have been more efficient than air-ice exchange in decreasing the difference of pCO₂ between SWR and SW due to bacterial respiration. This is in agreement with the higher Rayleigh

numbers observed at all times at the bottom of the growing sea ice, that indicate enhanced convection and therefore exchanges with the under-ice water.

Bacterial respiration in bulk ice ($10 \text{ nmolC L}^{-1} \text{ h}^{-1}$ in SW and $25 \text{ nmolC L}^{-1} \text{ h}^{-1}$) over 19 days only represent 1 to 3% of the stock of DIC ($400 \text{ } \mu\text{molC L}^{-1}$). It is therefore curious as to how such a low bacterial respiration may have caused a significant difference of pCO_2 in the ice interior. An explanation could be the increase of the buffering effect of the carbonate system with the decrease of temperature and the increase of salinity in brine (brine concentration). The chemical buffer factor ($\beta = \Delta\text{pCO}_2/\Delta\text{DIC}$) describes the change in pCO_2 relative to the DIC change induced by an input (i.e., respiration) or output of dissolved CO_2 . It results from the interplay of equilibrium dissociation reactions of the carbonate system and is a function of several physico-chemical conditions (Delille et al., 2005; Frankignoulle, 1994). In a closed system, β of brines increases significantly with decreasing temperature and the associated increase of brine salinity (Figure 8). Providing that bacterial respiration could explain the accumulation of DIC, an increase of DIC (even small) can result in a larger increase in pCO_2 in cold saline brine compared to warmer underlying seawater (Figure 8). Considering that the difference of DIC_7 in the ice interior approached $15 \text{ } \mu\text{mol kg}^{-1}$ (Figure 5) and that at β approached 4 at $-4.5 \text{ }^\circ\text{C}$ (median temperature of the ice), an expected difference of pCO_2 due to buffer factor changes should approach 60 ppm, which is relatively close to our observation (Figure 6).

An alternate explanation is the underestimation of the bacterial respiration in bulk ice. We calculated bacterial respiration based on thymidine incorporation and different conversion factors. Our choice of BGE might have led to an underestimation of the estimate of bacterial respiration, as discussed in the next section,.

4.4 Modelling the impact of bacterial respiration on pCO_2 in ice

In a closed system, bacterial respiration would induce an accumulation of DIC. In our semi-enclosed system, DIC also changed due to physical processes (ice-air and ice-water exchanges). The interplay of these various processes makes it difficult to use a simple calculation to prove (i) whether the difference in bacterial respiration caused the observed difference of DIC and pCO_2 in the ice interior, and (ii) whether ice-air and ice-water exchanges have offset the difference of DIC and pCO_2 caused by respiration at the surface and the bottom of the ice, respectively.

To tackle these issues, we used the one-dimensional thermodynamic sea ice model of Moreau et al. (2015) which includes ice-air gas exchanges and sea ice carbon dynamics. The model features ice growth and melt, ice-air and ice-water exchanges, as well as representations of full inorganic carbon and basic organic carbon dynamics within the ice. For the model simulations, all the parameters used are those described in Moreau et al. (2015), except for biological activity where primary production was shut down in the model runs. Bacterial respiration is prescribed with the median values of the bacterial respiration for SW and SWR, i.e., 10 nmol C L⁻¹ h⁻¹ in SW and 25 nmol C L⁻¹ h⁻¹ in SWR, which corresponded to the use of a bacterial growth efficiency (BGE) of 0.348. Based on the initial conditions of the experiment, we prescribed the initial seawater TA and DIC concentrations (2244 μmol kg⁻¹ and 2039 μmol kg⁻¹, respectively) and the initial sea ice TA and DIC concentrations (847 μmol kg⁻¹ and 748 μmol kg⁻¹). The model was run over 19 days (duration of the experiment), with a 1-hour time step.

Because the model has different temporal and spatial resolutions than the observations, we decided to only compare the temporal evolution of the median values in the ice (modelled versus measured variables). Overall, the model reproduced the ice thicknesses, median ice temperatures and salinities, as well as the standing stock of DIC and the median pCO₂ in ice in the same magnitude as those observed (Figure 9).

We first ran the model with the median values of the observed bacterial respiration for SW and SWR by using a BGE of 0.348 (Kuparinen et al., 2011). Given these bacterial respiration rates, the model reproduces the spatial pattern of the observed DIC₇ standing stock and the median pCO₂ (Figure 9) but not the magnitude of their difference between SW and SWR (Table 1). Therefore, we re-calculated bacterial respiration rates for SW and SWR using different BGE. Reducing BGE to 0.2 or 0.15 is plausible considering that BGE ranges from 0.05 to 0.6 (i.e., from 5 % to 60 %), depending on the environmental conditions (e.g., the quality of the dissolved organic matter) (Del Giorgio and Cole, 1998; Nguyen et al., 2012; Rivkin and Legendre, 2001).

Firstly, changing the BGE to 0.2 or 0.15, and hence increasing the BR, did not change the total stock of DIC and the median pCO₂ significantly (Figure 9, coloured curves), which supports our previous suggestions about the importance of the physical processes, such as brine concentration and dilution and gas transport, in regulating the dynamics of DIC and pCO₂ in sea ice. However, changing the BGE to 0.2 or 0.15 enhanced the differences in DIC₇ and pCO₂ in ice between SW and SWR (Table 1). The modelled median difference of DIC₇ fits the observations better when using a BGE of 0.2 and 0.15 (Table 1), and considering the reproducibility of +/- 0.8 μmol kg⁻¹ for DIC. The median difference of pCO₂ is then higher than

the observed differences in $p\text{CO}_2$ between SW and SWR, but considering that the model slightly overestimates the $p\text{CO}_2$ near the ice surface (*Kotovitch et al.*, submitted), differences in DIC_7 , rather than $p\text{CO}_2$, would be a better indicator of the difference in bacterial impact. The model simulations therefore suggest that the bacterial respiration in ice might be up to 3 times higher than our previous estimate (Table 1).

The estimate of BGE for the entire period of the experiment (0.15 - 0.2), as suggested by the model simulations, was lower than assumed. Our BGE estimate of 0.348 was based on empirical values obtained in liquid batch cultures in above-zero temperature (Kuparinen et al. 2011, Nguyen and Maranger 2011) combined with calculated temperature-dependent estimate (Rivkin & Legendre 2001). Measuring bacterial process rates, especially respiration in sea-ice systems is complicated and direct respiration measurements were not available. The lower actual BGE suggested by the model in our experimental system compared to the previous published values is plausible because of the extremely low temperatures and high salinities in brine. Extreme conditions are in general forcing bacteria to invest more energy for survival than for growth. Along these lines, the actual BGE may vary throughout the ice growth, being lower during ice growth (where the conditions were more extreme), and higher during ice melt (where the conditions were milder). Further investigations are encouraged to verify this hypothesis. Furthermore, BGE in water column and ice may be different with higher BGE in water where conditions are less extreme. Higher BGE from 0.4 to 0.5 were suggested by Moreau et al. (submitted) for the under-ice water, in the same experimental system. Higher BGE for under-ice water would also lower the respiration estimate towards values measured in other studies (Kirchman et al. 2009, Nguyen and Maranger 2011, Nguyen et al. 2012) albeit in the high Arctic under different nutrient and dissolved organic carbon regimes.

The comparison of Figure 5 with Figure 10, and Figure 6 with Figure 11 shows that the model reproduced the temporal and spatial pattern of DIC_7 and $p\text{CO}_2$ well. DIC_7 decreased from the bottom to the top of the ice due to air-ice gas exchange, except in the bottom most layer where DIC_7 is underestimated due to an improper parameterization of heat and salt transfer in this layer (Moreau et al., 2014; Vancoppenolle et al., 2010). $p\text{CO}_2$ was supersaturated in the ice during the entire ice growth period, except in the bottom layer where brine convection pulled the $p\text{CO}_2$ towards the under-saturated $p\text{CO}_2$ value of the under-ice water. $p\text{CO}_2$ in ice then also became under-saturated, as it was observed, as a result of the increase of air temperature (and the related brine dilution). In addition, due to the higher bacterial respiration in SWR compared to SW, DIC_7 and $p\text{CO}_2$ were higher in SWR than in SW. The differences of $p\text{CO}_2$ are alleviated

at the bottom of the ice because of brine convection, and slightly at the top of the ice due to air-ice gas exchange, but they are greater in the ice interior, which has to be associated with the difference in bacterial respiration – the sole difference between the two runs: SW and SWR.

There are two main differences between the model simulations and the observations: The absolute values of DIC_7 and pCO_2 are higher in the model than in the observations, and the differences of DIC_7 and pCO_2 between SWR and SW present a smoother pattern in the model than in the observations (Figures 5, 6, 9 and 10). Ice-air gas fluxes are currently not yet well constrained in the model, resulting in a slight underestimation of the ice-air gas fluxes, and thus an overestimation of the modeled DIC and pCO_2 content in the ice (Kotovitch et al., submitted). The smoother pattern in the modelled differences of DIC_7 and pCO_2 may result from the higher spatial and temporal resolution in the model than in the observations: Hourly time step and calculation on the 10 ice layers in the model compared to the almost daily sampling with 1 to 4 measured ice layers on each ice core.

In brief, differences exist between the model simulations and the observations, probably due to the parameterization of air-ice gas exchange and the difference of spatial and temporal resolution, but the model was able to reproduce the temporal and spatial patterns of DIC_7 and pCO_2 , confirming therefore the importance of brine concentration and dilution, and gas transport in controlling their dynamics. Most importantly, the model reproduced the observed median difference of DIC_7 in the ice by introducing the measured bacterial respiration (for a lower BGE of 0.15 or 0.2), confirming that higher bacterial respiration could indeed cause a larger accumulation of DIC and a larger pCO_2 in the ice.

A corollary to the higher bacterial respiration, DIC and pCO_2 in SWR in the model is an enhanced ice-air CO_2 flux during ice growth by 17 % ($1.68 \text{ mmol m}^{-2} \text{ d}^{-1}$ and $1.97 \text{ mmol m}^{-2} \text{ d}^{-1}$ in SW and SWR, respectively), and a reduced CO_2 flux during ice decay by 38 % ($-1.52 \text{ mmol m}^{-2} \text{ d}^{-1}$ and $-0.93 \text{ mmol m}^{-2} \text{ d}^{-1}$ in SW and SWR, respectively) if we assume a BGE of 0.15 (simulated fluxes not shown). The enhanced CO_2 fluxes during ice growth are obviously due to the higher pCO_2 in the ice resulting from the higher bacterial respiration. The negative CO_2 fluxes (i.e., from the air to the ice) are due to brine dilution (e.g., Nomura et al., 2010), and the flux is less negative in SWR because the larger bacterial respiration in SWR better compensates the effect of brine dilution. The integrated CO_2 flux over the 19 days of the simulation was $0.16 \text{ mmol m}^{-2} \text{ d}^{-1}$ and $1.04 \text{ mmol m}^{-2} \text{ d}^{-1}$ in SW and SWR, respectively. Hence, the addition of DOC might have induced an air-ice CO_2 flux that was more than 6 times higher than without the addition of DOC.

5. Conclusion and large scale implications

The aim of the study was to verify the hypothesis as to whether a larger input of riverine DOC in the Arctic water could induce a higher DOC concentration in sea ice, which would promote bacterial respiration, leading to a higher $p\text{CO}_2$ in brine. Although the overall trend of $p\text{CO}_2$ in both mesocosm series strongly depends on the ice temperature (Figure 1) as a result of the effect of brine concentration and brine dilution, the differences (SWR-SW) in observations and model simulations support our hypothesis.

The difference of $p\text{CO}_2$ between SW and SWR was much lower than the difference of $p\text{CO}_2$ in brine between the Arctic Ocean and the Southern Ocean. However, if we have added more labile DOC instead of humic-rich riverine water to our mesocosms and if we extended the duration of the experiment with lower air temperature, we may have observed larger differences of DIC and $p\text{CO}_2$, closer to those observed in natural conditions. The availability of more labile autochthonous DOC may promote higher bacterial respiration and higher accumulation of CO_2 in ice. Further, extending the duration of the experiment to several months, with further decrease of the ice temperature, would increase the respiration burden, reduce the ice permeability, and therefore reduce gases and DIC losses through the ice.

Because the addition of riverine DOC to seawater causes larger $p\text{CO}_2$ in ice, the Arctic Ocean, which receives a large input of terrestrial DOC through rivers, might induce more positive (or less negative) ice-air CO_2 fluxes than the Southern Ocean, for the same environmental conditions. Similarly, Arctic coastal waters might also be associated with a more positive (or negative) ice-air CO_2 fluxes than the central Arctic. This is at least true for the ice growth period when algal growth is limited, as considered by the absence of autochthonous DOC in our experiment. Algal growth would consume CO_2 but will also produce labile autochthonous DOC that enhances bacterial production. Further experiments are therefore needed to refine the net impact of algal and bacterial growth on $p\text{CO}_2$ in ice and on the inter-hemispheric differences.

The inter-hemispheric difference of $p\text{CO}_2$ in ice and brine likely results from the impact of ice temperature on the ice permeability and the buffering effect of the carbonate system, in addition to the DOC input. Lower ice temperatures are associated with larger buffering effects, i.e., the increase of $p\text{CO}_2$ in the ice interior in response to a given increase of DIC (due to bacterial respiration) would be enhanced. If the ice temperature is low enough so that the ice becomes impermeable to gas exchange, the accumulation of $p\text{CO}_2$ would have been more obvious, resulting in the larger observed inter-hemispheric difference of $p\text{CO}_2$ in ice and brine. On the contrary, higher ice temperatures are associated with lower buffering effects and larger ice

permeability. Exchange may occur through the ice, and offset the bacterial accumulation of CO_2 . In our study, the impact of bacterial respiration on pCO_2 was most obvious in the ice interior, because ice-air gas exchange and brine convection have offset the increase of pCO_2 associated with bacterial respiration at the ice interfaces.

Considering the drastic decline in Arctic sea ice, we may also wonder how air-sea and air-ice CO_2 fluxes may change in the future. If the ice cover is replaced more and more by open water, the most common scenario is that air-sea CO_2 fluxes increase, because gas exchange is more efficient via an open sea surface than a semi-permeable ice cover. Our work highlighted the fact that the dynamics regulating the pCO_2 gradient will be different too. Due to the buffering effect of the carbonate system, brine concentration makes the pCO_2 more sensitive to DIC increase in ice than in seawater, and a small accumulation of DIC, due to low bacterial respiration may result in a large increase of pCO_2 in the ice. At some specific locations, where bacterial activity is more intense in the ice than in the underlying water, the consequence of bacterial respiration on pCO_2 in ice may be even more significant, especially when algal activity is limited. The interplay between gas transfer velocity and the pCO_2 gradient needs to be taken into consideration while assessing the future evolution of the air-sea and air-ice CO_2 fluxes in the polar regions.

Acknowledgments

We are grateful to two anonymous reviewers for their useful comments which have improved the quality of the manuscript. This study was supported by the European Community's 7th Framework Programme through the grant to the budget of the Integrated Infrastructure Initiative HYDRALAB-IV, Contract no. 261520. The authors would like to thank the Hamburg Ship Model Basin (HSVA), Karl-Ulrich Evers and the rest of the ice tank crew, for the hospitality, technical and scientific support and the professional execution of the test program in the Research Infrastructure ARCTICLAB. The work was supported by a FiDiPro award by the Academy of Finland, the Walter and Andree Nottbeck Foundation, and the BIGSOUTH project funded by the Belgian Science Federal Policy Office. MK, SM and BD are respectively research fellows, postdoctoral researcher and research associate of the Fonds de la Recherche Scientifique –FNRS. JZ was a F.R.S.-FNRS research fellow and is presently a BAEF Francqui Foundation research fellow. This is a MARE contribution n°XXX.

Contributions

708 JLT, BD, GD, HK, GK planned and designed the experiment under the lead of DT; JZ, MK,
709 JLT, BD, GD and DT provided the data on sea ice physics and carbonate chemistry, HK, the
710 bacterial data, GK, the DOC data, and SM, the model simulations. JZ, BD, HK, SM wrote the
711 paper with the valuable comments and inputs from all the other co-authors.

712

Captions

Figure 1. pCO₂ measurements in sea ice and brine in the Arctic and Antarctica after Geilfus et al. (2014), excluding the measurements where flooding was observed. The horizontal line indicates a pCO₂ of 400ppm - a reference value considering current atmospheric pCO₂.

Figure 2. Brine volume fraction (BrV, in %) and Rayleigh number (Ra) in the SW and SWR mesocosms during the experiment. The black dots are the data points from the sampling, while the color in between results is from interpolation (natural neighbours in Surfer 8 © software) (Zhou et al., 2014).

Figure 3. a) Bacterial respiration (BR_TdR), b) DIC₇ and c) pCO₂ in water and sea ice. Note that for sea ice, we plotted the median value of each ice core.

Figure 4. Bacterial respiration (BR_TdR) in ice in the SW and SWR mesocosms during the experiment, and the difference between both mesocosms. Bacterial respiration is expressed in nmol C L⁻¹ h⁻¹.

Figure 5. DIC₇ in ice of the SW and SWR mesocosms during the experiment, and the difference between both mesocosms. DIC₇ is expressed in μmol C kg⁻¹. Insignificant differences of DIC₇ are set in white.

Figure 6. pCO₂ in ice in the SW and SWR mesocosms during the experiment, and the difference between both mesocosms. pCO₂ is expressed in ppm. Insignificant differences of pCO₂ are set in white.

Figure 7. Relationship between pCO₂ in ice and brine volume fraction. The circles are the data used to draw the fit (black curve), the other discrete symbols are not considered (see explanation in the text). The blue curves are the 95 % confidence bands of the fit and the red dashed curve is the relationship predicted by CO2SYS (Lewis and Wallace, 1998).

Figure 8. Buffer factor of the carbonate system for decreasing temperature and related increase of salinity due to brine concentration/dilution in a closed system. Initial conditions was S = 35.17, T = -1.8 °C, TA = 2578 μmol kg⁻¹, DIC = 2450.4 μmol kg⁻¹, pCO₂ = 400 μatm. β is provided for an increase of DIC of 20 μmol kg⁻¹.

Figure 9. (Clockwise) Temporal changes of the ice thickness, median ice temperature, median ice salinity, the standing stock of DIC and the median pCO₂ in the ice. The dots refer to the measurements (white for SW and black for SWR), while the curves refer to the simulated results. The vertical dashed line shows the transition from ice growth to ice decay.

Figure 10 Modeled DIC₇ in ice, in SW and SWR mesocosms, and the difference SWR minus SW, using a median bacterial respiration in ice associated with a BGE of 0.15 (Table 1).

Figure 11. Modeled pCO₂ in ice, in SW and SWR mesocosms, and the difference SWR minus SW, using a median bacterial respiration in ice associated with a BGE of 0.15 (Table 1).

Table 1. Calculated median bacterial respiration (BR) in ice in SW and SWR using different bacterial growth efficiencies (BGE), the measured median difference of pCO₂ and DIC (SWR minus SW) during the experiment (Diff pCO₂ and Diff DIC₇), and the modeled difference of pCO₂ and DIC for each set of BGE-dependent BR.

References

- Anderson, G.M., 1976. Error propagation by the Monte Carlo method in geochemical calculations. *Geochim. Cosmochim. Acta* 40, 1533–1538.
- Aslam, S.N., Underwood, G.J.C., Kaartokallio, H., Norman, L., Autio, R., Fischer, M., Kuosa, H., Dieckmann, G.S., Thomas, D.N., 2012. Dissolved extracellular polymeric substances (dEPS) dynamics and bacterial growth during sea ice formation in an ice tank study. *Polar Biol.* 35, 661–676. doi:10.1007/s00300-011-1112-0
- Baer, S., Connelly, T., Bronk, D., 2015. Nitrogen uptake dynamics in landfast sea ice of the Chukchi Sea. *Polar Biol.* 38, 781–797. doi:10.1007/s00300-014-1639-y
- Brown, K.A., Miller, L.A., Davelaar, M., Francois, R., Tortell, P.D., 2014. Overdetermination of the carbonate system in natural sea-ice brine and assessment of carbonic acid dissociation constants under low temperature, high salinity conditions. *Mar. Chem.* 165, 36–45. doi:10.1016/j.marchem.2014.07.005
- Copin-Montegut, C., 1988. A new formula for the effect of temperature on the partial pressure of CO₂ in seawater. *Mar. Chem.* 25, 29–37. doi:10.1016/0304-4203(88)90012-6
- Cox, G.F.N., Weeks, W.F., 1983. Equations for determining the gas and brine volumes in sea ice samples. *J. Glaciol.* 29, 306–316.
- Crabeck, O., Delille, B., Thomas, D., Geilfus, N.-X., Rysgaard, S., Tison, J.-L., 2014. CO₂ and CH₄ in sea ice from a subarctic fjord under influence of riverine input. *Biogeosciences* 11, 6525–6538. doi:10.5194/bg-11-6525-2014
- Del Giorgio, P., Cole, J.J., 1998. Bacterial growth efficiency in natural aquatic systems. *Annu. Rev. Ecol. Syst.* 29, 503–541.
- Delille, B., 2006. Inorganic carbon dynamics and air-ice-sea CO₂ fluxes in the open and coastal waters of the Southern Ocean. Université de Liège, Belgique.
- Delille, B., Harlay, J., Zondervan, I., Jacquet, S., Chou, L., Wollast, R., Bellerby, R.G.J., Frankignoulle, M., Borges, A.V., Riebesell, U., Gattuso, J.P., 2005. Response of primary production and calcification to changes of pCO₂ during experimental blooms of the coccolithophorid *Emiliana huxleyi*. *Global Biogeochem. Cycles* 19, 1–14. doi:10.1029/2004GB002318
- Delille, B., Jourdain, B., Borges, A. V., Tison, J.-L., Delille, D., 2007. Biogas (CO₂, O₂, dimethylsulfide) dynamics in spring Antarctic fast ice. *Limnol. Oceanogr.* 52, 1367–1379. doi:10.4319/lo.2007.52.4.1367
- Delille, B., Vancoppenolle, M., Geilfus, N.-X., Tilbrook, B., Lannuzel, D., Schoemann, V., Becquevort, S., Carnat, G., Delille, D., Lancelot, C., Chou, L., Dieckmann, G.S., Tison, J.-L., 2014. Southern Ocean CO₂ sink: The contribution of the sea ice. *J. Geophys. Res. Ocean.* 119, 6340–6355. doi:10.1002/2014JC009941

- 789 Dickson, A.G., Millero, F.J., 1987. A comparison of the equilibrium constants for the
790 dissociation of carbonic acid in seawater media. *Deep Sea Res.* 34, 1733–1743.
791 doi:10.1016/0198-0149(87)90021-5
- 792 Dieckmann, G.S., Nehrke, G., Papadimitriou, S., Göttlicher, J., Steininger, R., Kennedy, H.,
793 Wolf-Gladrow, D., Thomas, D.N., 2008. Calcium carbonate as ikaite crystals in
794 Antarctic sea ice. *Geophys. Res. Lett.* 35, 35–37. doi:10.1029/2008GL033540
- 795 Dieckmann, G.S., Nehrke, G., Uhlig, C., Göttlicher, J., Gerland, S., Granskog, M.A., Thomas,
796 D.N., 2010. Brief Communication: Ikaite ($\text{CaCO}_3 \cdot 6\text{H}_2\text{O}$) discovered in Arctic sea ice.
797 *Cryosphere* 4, 227–230. doi:10.5194/tc-4-227-2010
- 798 Dittmar, T., Kattner, G., 2003. The biogeochemistry of the river and shelf ecosystem of the
799 Arctic Ocean: a review. *Mar. Chem.* 83, 103–120. doi:10.1016/S0304-4203(03)00105-1
- 800 DOE, 1994. Handbook of Methods for the Analysis of the Various Parameters of the Carbon
801 Dioxide System in Sea Water; version2.
- 802 Eronen-Rasimus, E., Kaartokallio, H., Lyra, C., Autio, R., Kuosa, H., Dieckmann, G.S.,
803 Thomas, D.N., 2014. Bacterial community dynamics and activity in relation to dissolved
804 organic matter availability during sea-ice formation in a mesocosm experiment.
805 *Microbiologyopen* 3, 139–156. doi:10.1002/mbo3.157
- 806 Frankignoulle, M., 1994. A complete set of buffer factors for acid/base CO_2 system in
807 seawater. *J. Mar. Syst.* 5, 111–118. doi:10.1016/0924-7963(94)90026-4
- 808 Fuhrman, J.A., Azam, F., 1982. Thymidine incorporation as a measure of heterotrophic
809 bacterioplankton production in marine surface waters: Evaluation and field results. *Mar.*
810 *Biol.* 66, 109–120. doi:10.1007/BF00397184
- 811 Fuhrman, J.A., Azam, F., 1980. Bacterioplankton secondary production estimates for coastal
812 waters of British Columbia, Antarctica, and California. *Appl. Environ. Microbiol.* 39,
813 1085–1095.
- 814 Geilfus, N.-X., Carnat, G., Dieckmann, G.S., Halden, N., Nehrke, G., Papakyriakou, T.,
815 Tison, J.-L., Delille, B., 2013. First estimates of the contribution of CaCO_3 precipitation
816 to the release of CO_2 to the atmosphere during young sea ice growth. *J. Geophys. Res.*
817 *Ocean.* 118, 244–255. doi:10.1029/2012JC007980
- 818 Geilfus, N.-X., Carnat, G., Papakyriakou, T., Tison, J.-L., Else, B., Thomas, H., Shadwick, E.,
819 Delille, B., 2012a. Dynamics of pCO_2 and related air-ice CO_2 fluxes in the Arctic
820 coastal zone (Amundsen Gulf, Beaufort Sea). *J. Geophys. Res. Ocean.* 117, C00G10.
821 doi:10.1029/2011JC007118
- 822 Geilfus, N.-X., Delille, B., Verbeke, V., Tison, J.-L., 2012b. Towards a method for high
823 vertical resolution measurements of the partial pressure of CO_2 within bulk sea ice. *J.*
824 *Glaciol.* 58, 287–300. doi:10.3189/2012JoG11J071
- 825 Geilfus, N.-X., Tison, J.-L., Ackley, S.F., Galley, R.J., Rysgaard, S., Miller, L.A., Delille, B.,
826 2014. Sea ice pCO_2 dynamics and air-ice CO_2 fluxes during the Sea Ice Mass Balance in

- 827 the Antarctic (SIMBA) experiment – Bellingshausen Sea, Antarctica. *Cryosph.* 8, 2395–
828 2407. doi:10.5194/tc-8-2395-2014
- 829 Giannelli, V., Thomas, D.N., Haas, C., Kattner, G., Kennedy, H., Dieckmann, G.S., 2001.
830 Behaviour of dissolved organic matter and inorganic nutrients during experimental sea-
831 ice formation. *Ann. Glaciol.* 33, 317–321. doi:10.3189/172756401781818572
- 832 Golden, K.M., Ackley, S.F., Lytle, V.I., 1998. The percolation phase transition in sea ice.
833 *Science* (80-.). 282, 2238–2241. doi:10.1126/science.282.5397.2238
- 834 Gosink, T.A., Pearson, J.G., Kelley, J.J., 1976. Gas movement through sea ice. *Nature* 263,
835 41–42.
- 836 Goyet, C., Poisson, A., 1989. New determination of carbonic acid dissociation constants in
837 seawater as a function of temperature and salinity. *Deep Sea Res.* 36, 1635–1654.
838 doi:10.1016/0198-0149(89)90064-2
- 839 Gran, G., 1952. Determination of the Equivalence Point in Potentiometric Titrations. Part II.
840 *Analyst* 77, 661–671.
- 841 Hansell, D., Carlson, C., Repeta, D., Schlitzer, R., 2009. Dissolved Organic Matter in the
842 Ocean: A Controversy Stimulates New Insights. *Oceanography*.
843 doi:10.5670/oceanog.2009.109
- 844 Helmke, E., Weyland, H., 1995. Bacteria in sea ice and underlying water of the eastern
845 Weddell Sea in midwinter. *Mar. Ecol. Prog. Ser.* 117, 269–288.
846 doi:10.3354/meps117269
- 847 Hunke, E.C., Notz, D., Turner, A.K., Vancoppenolle, M., 2011. The multiphase physics of sea
848 ice: a review for model developers. *Cryosph.* 5, 989–1009. doi:10.5194/tc-5-989-2011
- 849 Jørgensen, L., Stedmon, C. a., Kaartokallio, H., Middelboe, M., Thomas, D.N., 2015.
850 Changes in the composition and bioavailability of dissolved organic matter during sea
851 ice formation. *Limnol. Oceanogr.* 00, 00–00. doi:10.1002/lno.10058
- 852 Kaartokallio, H., 2004. Food web components, and physical and chemical properties of Baltic
853 Sea ice. *Mar. Ecol. Prog. Ser.* 273, 49–63. doi:10.3354/meps273049
- 854 Kirchman, D.L., Hill, V., Cottrell, M.T., Gradinger, R., Malmstrom, R.R., Parker, A., 2009.
855 Standing stocks, production, and respiration of phytoplankton and heterotrophic bacteria
856 in the western Arctic Ocean. *Deep. Res. Part II Top. Stud. Oceanogr.* 56, 1237–1248.
857 doi:10.1016/j.dsr2.2008.10.018
- 858 Kotovitch, M., Moreau, S., Zhou, J., Goosse, H., Vancoppenolle, M., Dieckmann, G.S.,
859 Thomas, D.N., Tison, J.-L., Delille, B., n.d. Measurements of air-ice CO₂ fluxes over
860 experimental sea ice emphasize the role of bubbles in gas transport during ice growth,
861 *Elementa: Science of the Anthropocene*.

862 Krembs, C., Eicken, H., Deming, J.W., 2011. Exopolymer alteration of physical properties of
863 sea ice and implications for ice habitability and biogeochemistry in a warmer Arctic.
864 Proc. Natl. Acad. Sci. U. S. A. 108, 3653–8. doi:10.1073/pnas.1100701108

865 Kuparinen, J., Autio, R., Kaartokallio, H., 2011. Sea ice bacterial growth rate, growth
866 efficiency and preference for inorganic nitrogen sources in the Baltic Sea. Polar Biol. 34,
867 1361–1373. doi:10.1007/s00300-011-0989-y

868 Lewis, E., Wallace, D.W.R., 1998. Program developed for CO₂ system calculations.

869 Loose, B., McGillis, W.R., Perovich, D., Zappa, C.J., Schlosser, P., 2014. A parameter model
870 of gas exchange for the seasonal sea ice zone. Ocean Sci. 10, 17–28. doi:10.5194/os-10-
871 17-2014

872 Loose, B., Schlosser, P., Perovich, D., Ringelberg, D., Ho, D.T., Takahashi, T., Richter-
873 Menge, J., Reynolds, C.M., McGillis, W.R., Tison, J.-L., 2011. Gas diffusion through
874 columnar laboratory sea ice: implications for mixed-layer ventilation of CO₂ in the
875 seasonal ice zone. Tellus B 63, 23–39. doi:10.1111/j.1600-0889.2010.00506.x

876 Marion, G.M., 2001. Carbonate mineral solubility at low temperatures in the Na-K-Mg-Ca-H-
877 Cl-SO₄-OH-HCO₃-CO₃-CO₂-H₂O system. Geochim. Cosmochim. Acta 65, 1883–
878 1896.

879 Mehrbach, C., Culbrtton, C.H., Hawley, J.E., Pytkowicz, R.M., 1973. Measurement of the
880 apparent dissociation constants of carbonic acid in seawater at atmospheric pressure.
881 Limnol. Oceanogr. 18, 897–907. doi:10.4319/lo.1973.18.6.0897

882 Miller, L.A., Carnat, G., Else, B.G.T., Sutherland, N., Papakyriakou, T.N., 2011a. Carbonate
883 system evolution at the Arctic Ocean surface during autumn freeze-up. J. Geophys. Res.
884 116, C00G04. doi:10.1029/2011JC007143

885 Miller, L.A., Papakyriakou, T.N., Collins, R.E., Deming, J.W., Ehn, J.K., Macdonald, R.W.,
886 Mucci, A., Owens, O., Raudsepp, M., Sutherland, N., 2011b. Carbon dynamics in sea
887 ice: A winter flux time series. J. Geophys. Res. 116, C02028.
888 doi:10.1029/2009JC006058

889 Moreau, S., Kaartokallio, H., Vancoppenolle, M., Zhou, J., Kotovitch, M., Dieckmann, G.S.,
890 Thomas, D.N., Goosse, H., Tison, J.-L., Delille, B., n.d. Closing the O₂ and CO₂ budget
891 under a growing ice sheet - a laboratory investigation, Elementa: Science of the
892 Anthropocene.

893 Moreau, S., Vancoppenolle, M., Delille, B., Tison, J.-L., Zhou, J., Kotovitch, M., Thomas,
894 D.N., Geilfus, N.-X., Goosse, H., 2015. Drivers of inorganic carbon dynamics in first-
895 year sea ice: A model study. J. Geophys. Res. Ocean. 120, 471–495.
896 doi:10.1002/2014JC010388

897 Moreau, S., Vancoppenolle, M., Zhou, J., Tison, J.-L., Delille, B., Goosse, H., 2014.
898 Modelling argon dynamics in first-year sea ice. Ocean Model. 73, 1–18.
899 doi:10.1016/j.ocemod.2013.10.004

- 900 Müller, S., Vähätalo, A. V., Stedmon, C. a., Granskog, M. a., Norman, L., Aslam, S.N.,
 901 Underwood, G.J.C., Dieckmann, G.S., Thomas, D.N., 2013. Selective incorporation of
 902 dissolved organic matter (DOM) during sea ice formation. *Mar. Chem.* 155, 148–157.
 903 doi:10.1016/j.marchem.2013.06.008
- 904 Nagata, T., Watanabe, Y., 1990. Carbon- and nitrogen-to-volume ratios of bacterioplankton
 905 grown under different nutritional conditions. *Appl. Environ. Microbiol.* 56, 1303–1309.
- 906 Nguyen, D., Maranger, R., 2011. Respiration and bacterial carbon dynamics in Arctic sea ice.
 907 *Polar Biol.* 34, 1843–1855. doi:10.1007/s00300-011-1040-z
- 908 Nguyen, D., Maranger, R., Tremblay, J.É., Gosselin, M., 2012. Respiration and bacterial
 909 carbon dynamics in the Amundsen Gulf, western Canadian Arctic. *J. Geophys. Res.*
 910 *Ocean.* 117, 1–12. doi:10.1029/2011JC007343
- 911 Nomura, D., Eicken, H., Gradinger, R., Shirasawa, K., 2010. Rapid physically driven
 912 inversion of the air–sea ice CO₂ flux in the seasonal landfast ice off Barrow, Alaska after
 913 onset of surface melt. *Cont. Shelf Res.* 30, 1998–2004. doi:10.1016/j.csr.2010.09.014
- 914 Notz, D., Worster, M.G., 2009. Desalination processes of sea ice revisited. *J. Geophys. Res.*
 915 114, C05006. doi:10.1029/2008JC004885
- 916 Notz, D., Worster, M.G., 2008. In situ measurements of the evolution of young sea ice. *J.*
 917 *Geophys. Res. Ocean.* 113, C03001. doi:10.1029/2007JC004333
- 918 Papadimitriou, S., Thomas, D.N., Kennedy, H., Haas, C., Kuosa, H., Krell, A., Dieckmann,
 919 G.S., 2007. Biogeochemical composition of natural sea ice brines from the Weddell Sea
 920 during early austral summer. *Limnol. Oceanogr.* 52, 1809–1823.
 921 doi:10.4319/lo.2007.52.5.1809
- 922 Pelegrí, S.P., Dolan, J., Rassoulzadegan, F., 1999. Use of high temperature catalytic oxidation
 923 (HTCO) to measure carbon content of microorganisms. *Aquat. Microb. Ecol.* 16, 273–
 924 280. doi:10.3354/ame016273
- 925 Rivkin, R.B., Legendre, L., 2001. Biogenic carbon cycling in the upper ocean: effects of
 926 microbial respiration. *Science* (80-.). 291, 2398–2400.
- 927 Rysgaard, S., Glud, R.N., Sejr, M.K., Bendtsen, J., Christensen, P.B., 2007. Inorganic carbon
 928 transport during sea ice growth and decay: A carbon pump in polar seas. *J. Geophys.*
 929 *Res.* 112, C03016. doi:10.1029/2006JC003572
- 930 Shadwick, E.H., Thomas, H., Chierici, M., Else, B., Fransson, A., Michel, C., Miller, L.A.,
 931 Mucci, A., Niemi, A., Papakyriakou, T.N., Tremblay, J.-É., 2011. Seasonal variability of
 932 the inorganic carbon system in the Amundsen Gulf region of the southeastern Beaufort
 933 Sea. *Limnol. Oceanogr.* 56, 303–322. doi:10.4319/lo.2011.56.1.0303
- 934 Smith, R.E.H., Clement, P., 1990. Heterotrophic activity and bacterial productivity in
 935 assemblages of microbes from sea ice in the high Arctic. *Polar Biol.* 10, 351–357.
 936 doi:10.1007/BF00237822

937 Vancoppenolle, M., Goosse, H., de Montety, A., Fichefet, T., Tremblay, B., Tison, J.-L.,
938 2010. Modeling brine and nutrient dynamics in Antarctic sea ice: The case of dissolved
939 silica. *J. Geophys. Res.* 115, C02005. doi:10.1029/2009JC005369

940 Zhou, J., Delille, B., Eicken, H., Vancoppenolle, M., Brabant, F., Carnat, G., Geilfus, N.-X.,
941 Papakyriakou, T., Heinesch, B., Tison, J.-L., 2013. Physical and biogeochemical
942 properties in landfast sea ice (Barrow, Alaska): Insights on brine and gas dynamics
943 across seasons. *J. Geophys. Res. Ocean.* 118, 3172–3189. doi:10.1002/jgrc.20232

944 Zhou, J., Delille, B., Kaartokallio, H., Kattner, G., Kuosa, H., Tison, J.-L., Autio, R.,
945 Dieckmann, G.S., Evers, K.-U., Jørgensen, L., Kennedy, H., Kotovitch, M., Luhtanen,
946 A.-M., Stedmon, C.A., Thomas, D.N., 2014. Physical and bacterial controls on inorganic
947 nutrients and dissolved organic carbon during a sea ice growth and decay experiment.
948 *Mar. Chem.* 166, 59–69. doi:10.1016/j.marchem.2014.09.013

949

950

951

952

	Observations				Model	
	BR (SW)	BR (SWR)	Diff pCO ₂	Diff DIC ₇	Diff pCO ₂	Diff DIC ₇
	nmol C L ⁻¹ h ⁻¹	nmol C L ⁻¹ h ⁻¹	ppm	μmol kg ⁻¹	ppm	μmol kg ⁻¹
BGE = 0.348	10.0	24.7	13	2.8	8.3	0.9
BGE = 0.2	21.5	52.6			19.3	1.9
BGE = 0.15	30.4	74.6			31.9	2.7

Fig. 1

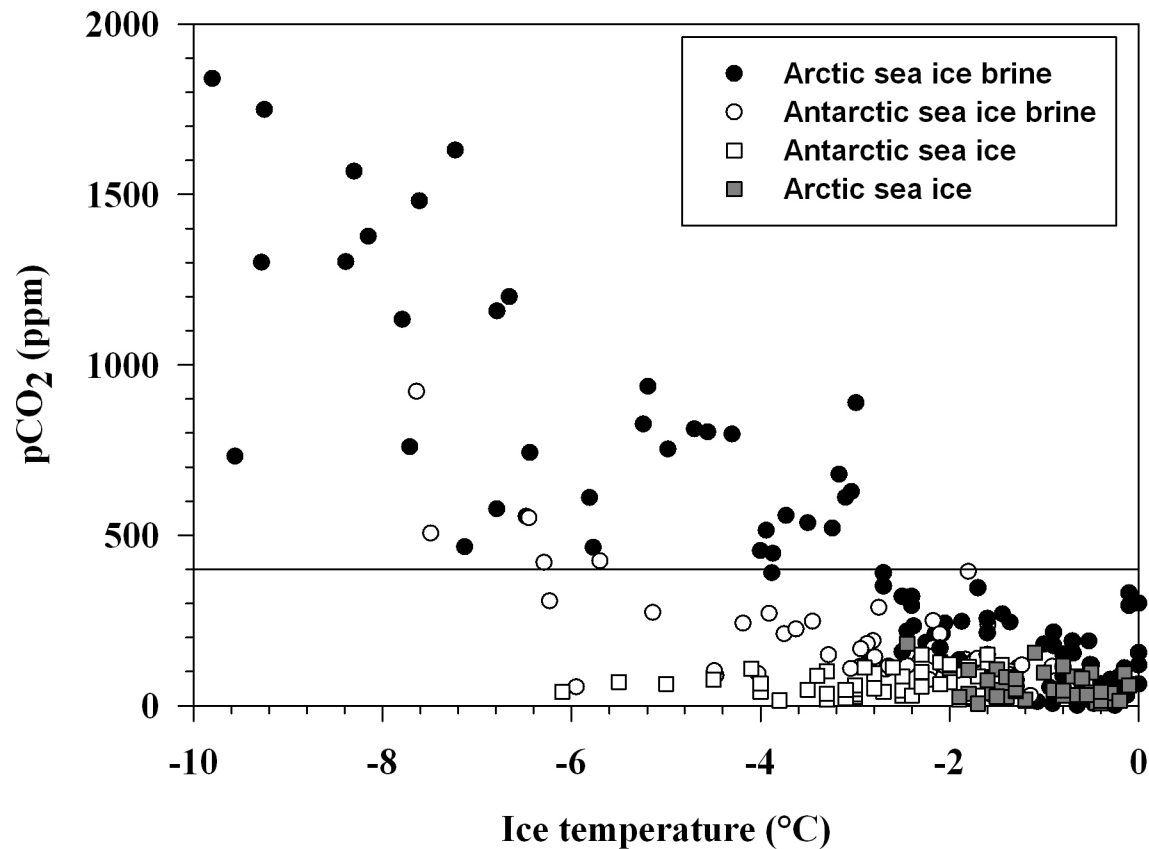


Fig. 2

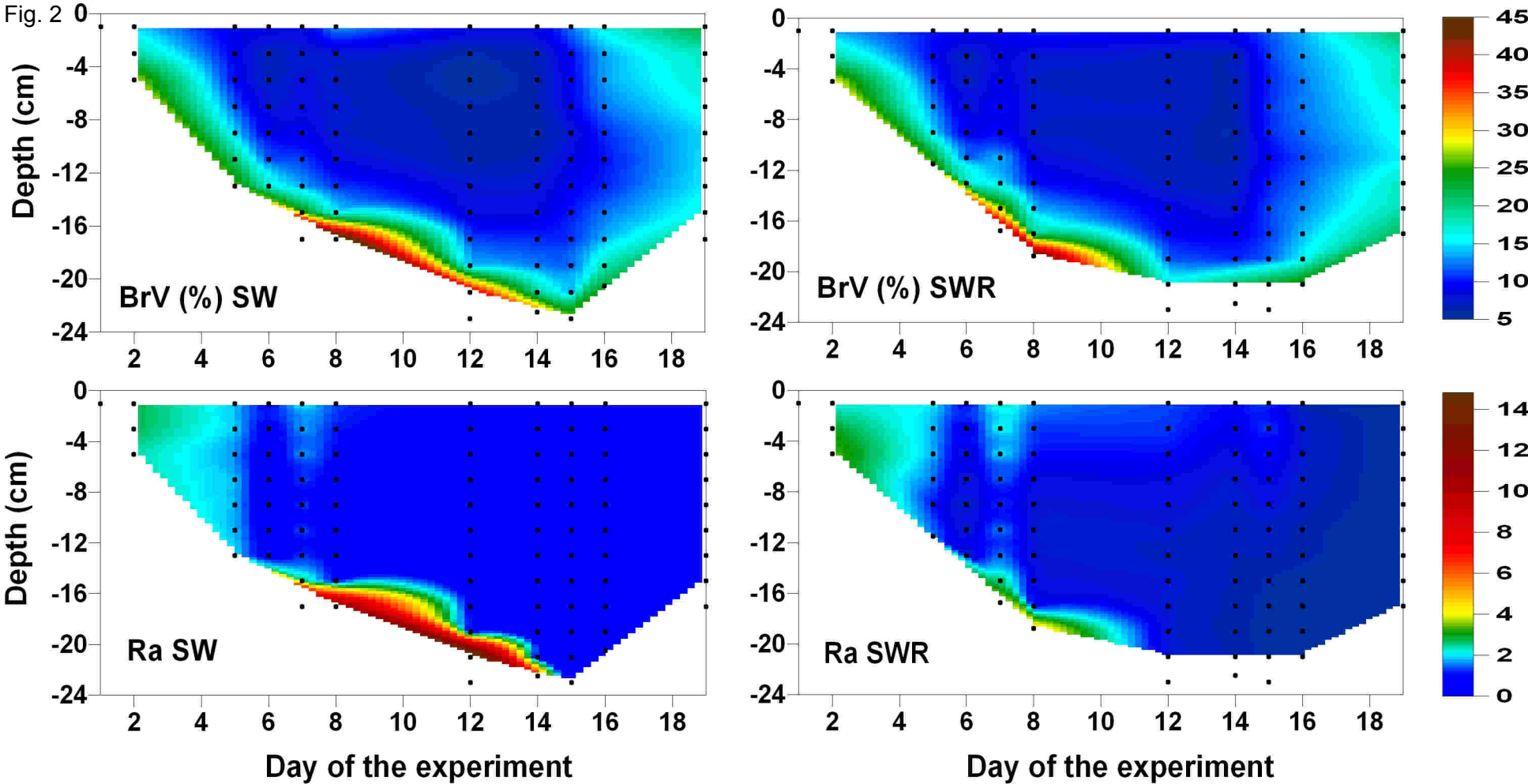


Fig.3

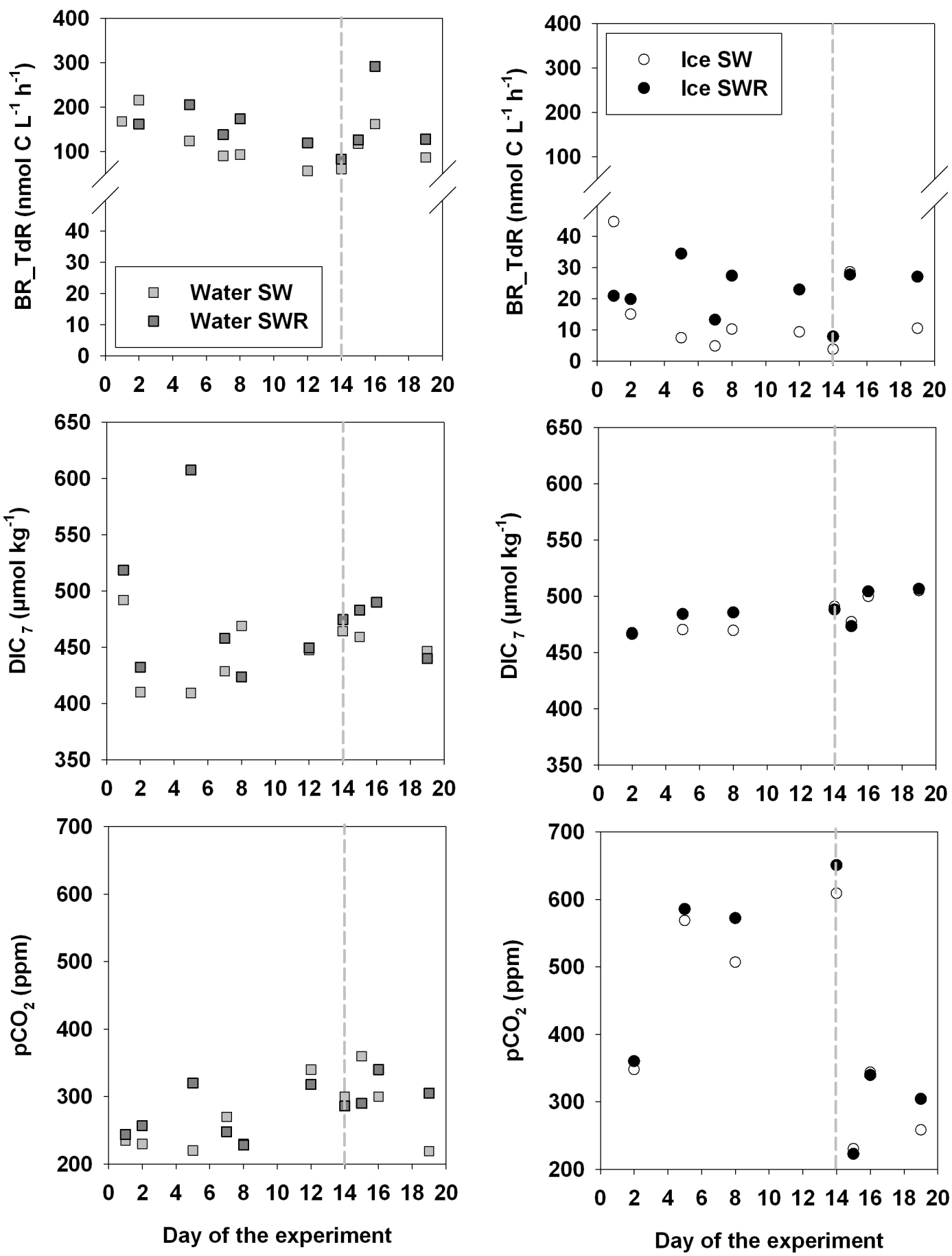


Fig. 4

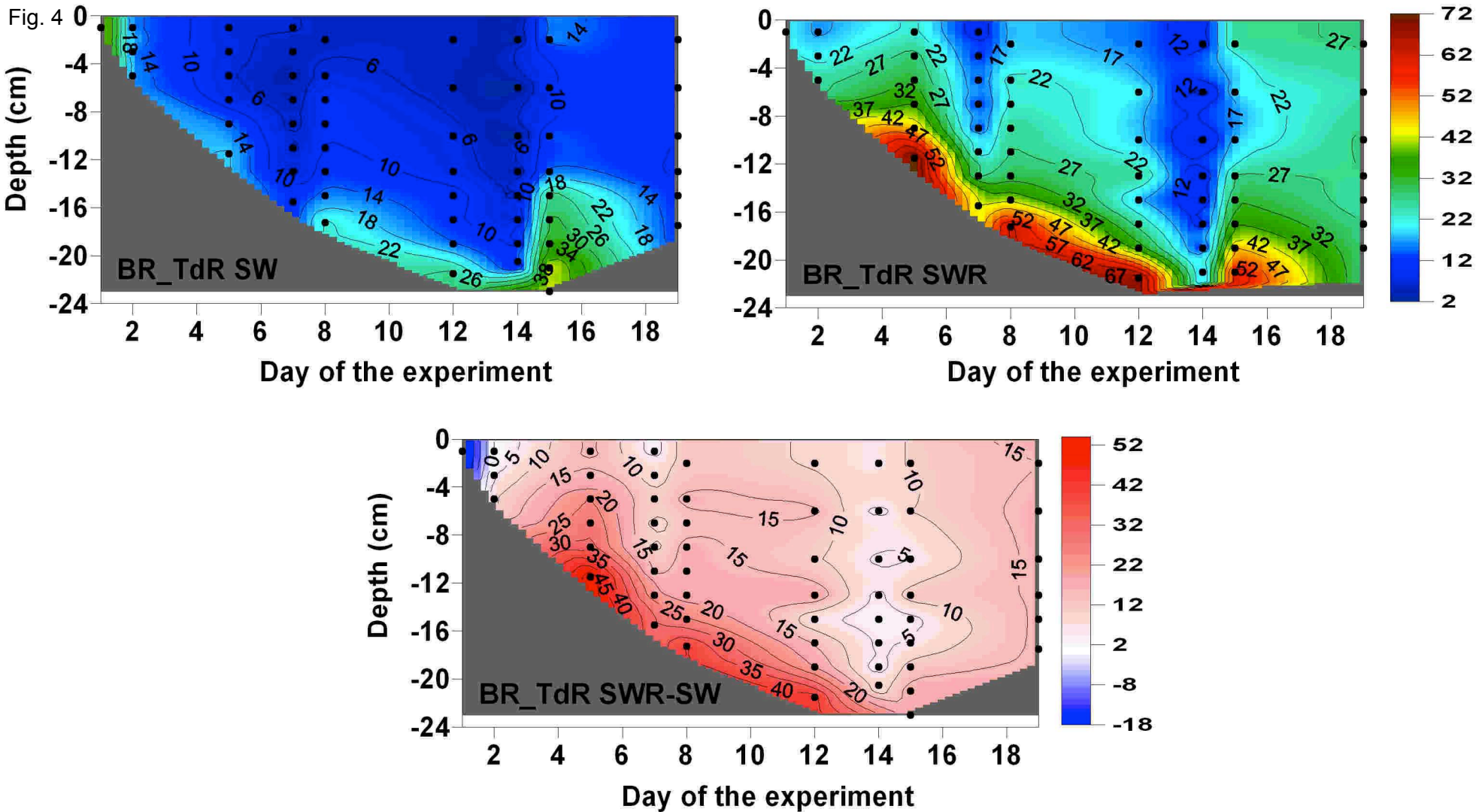


Fig. 5

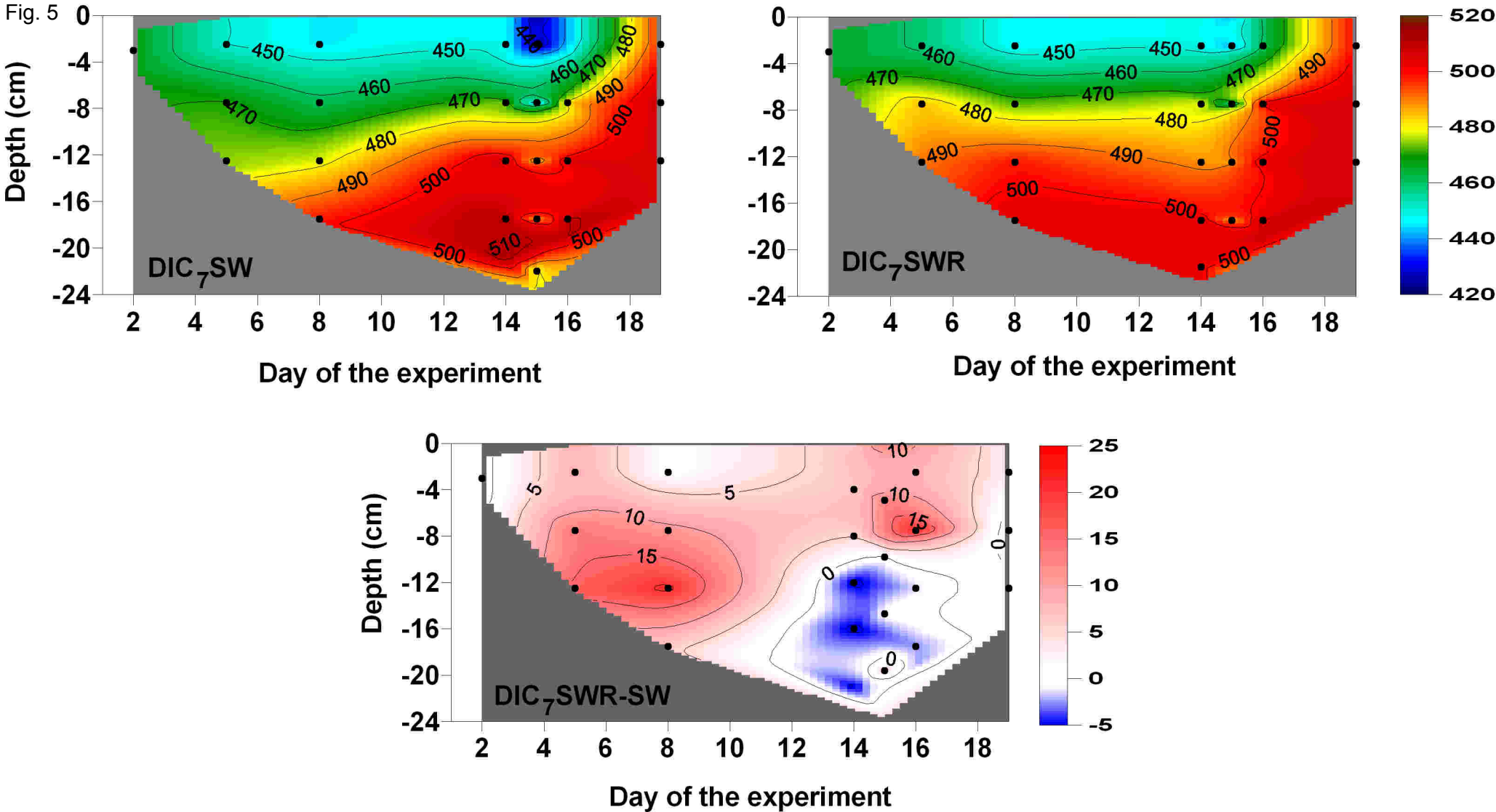


Fig. 6

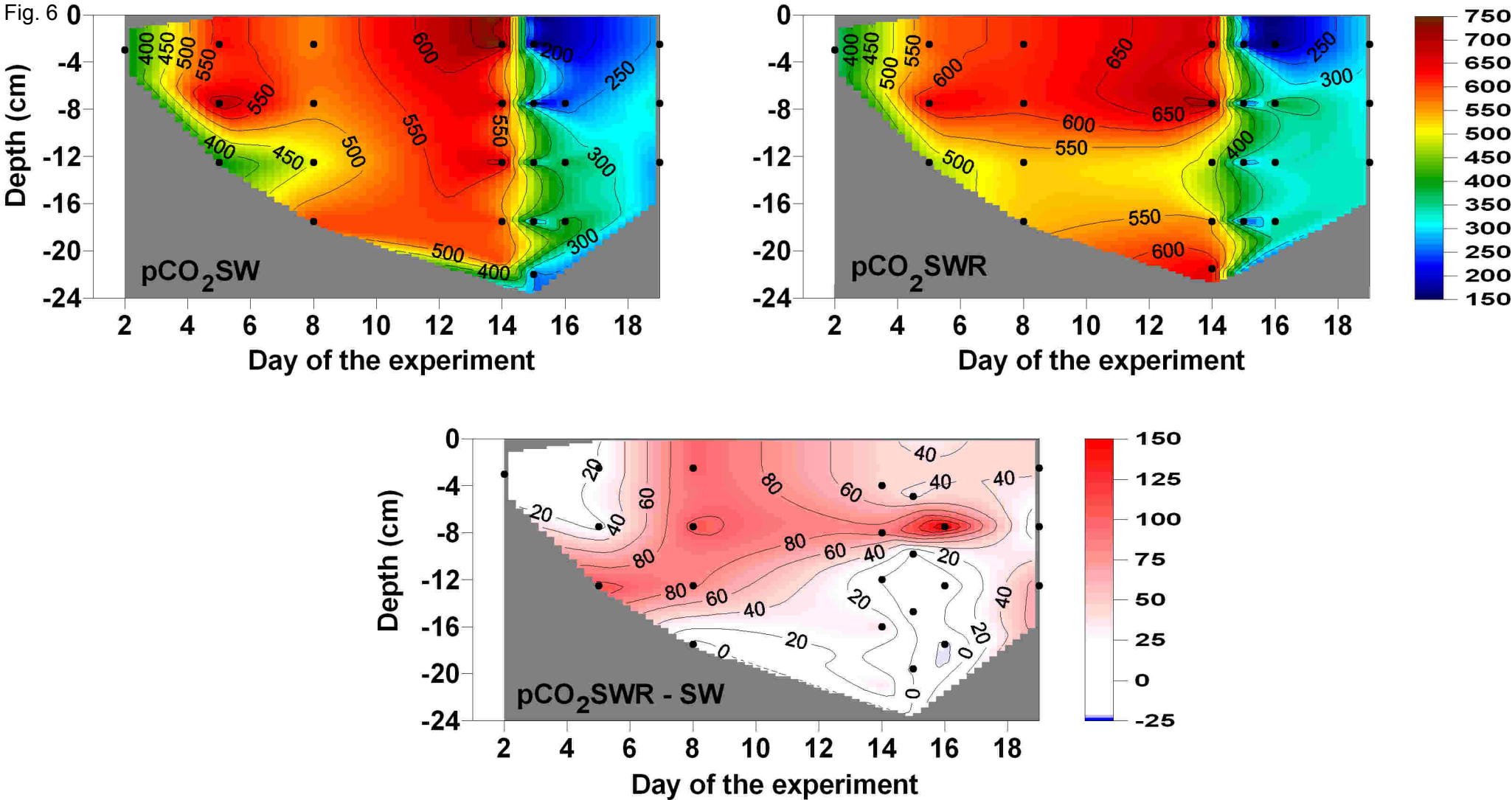


Fig. 7

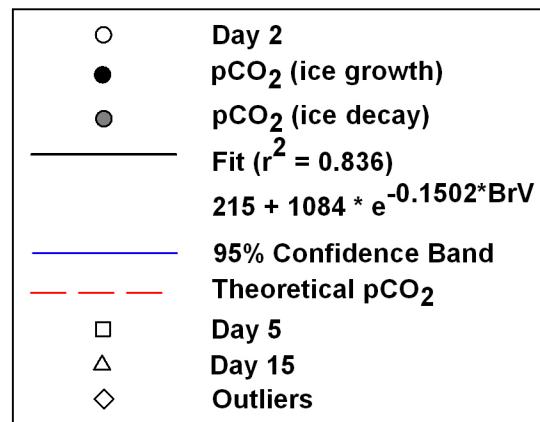
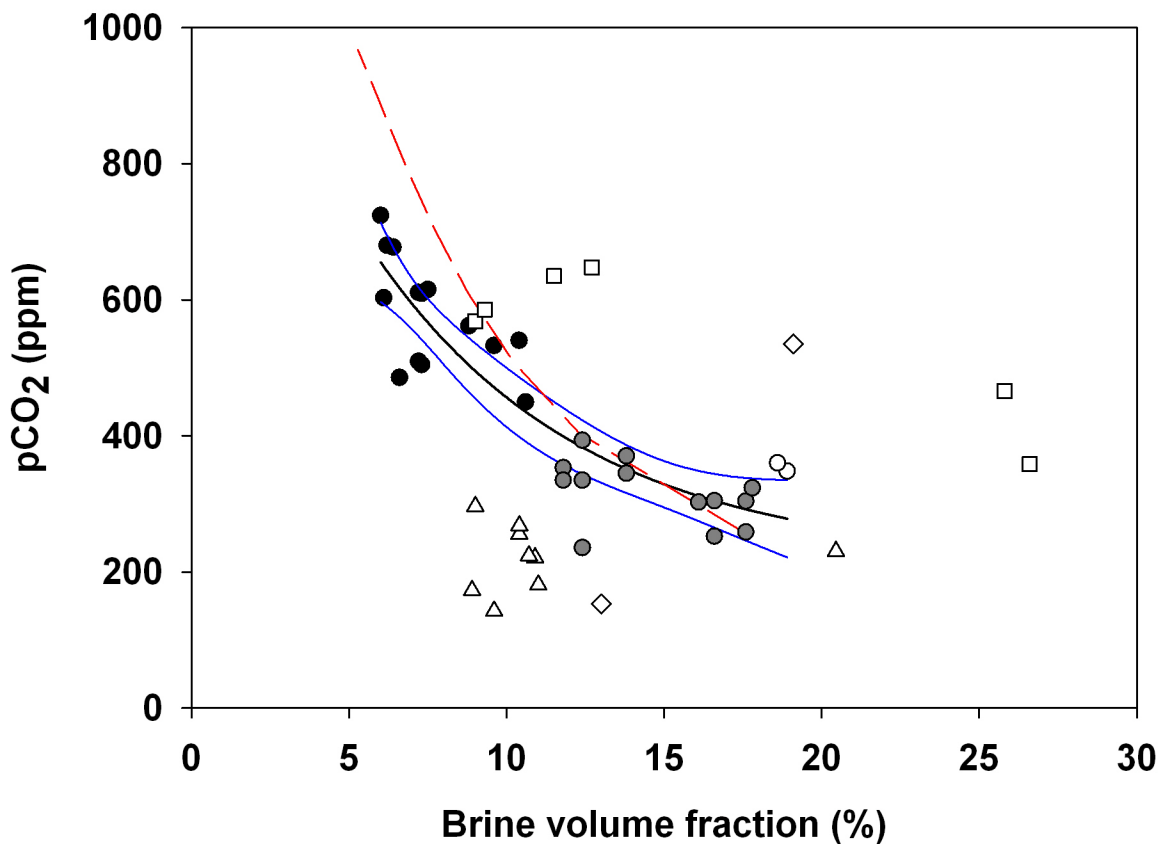


Fig. 8

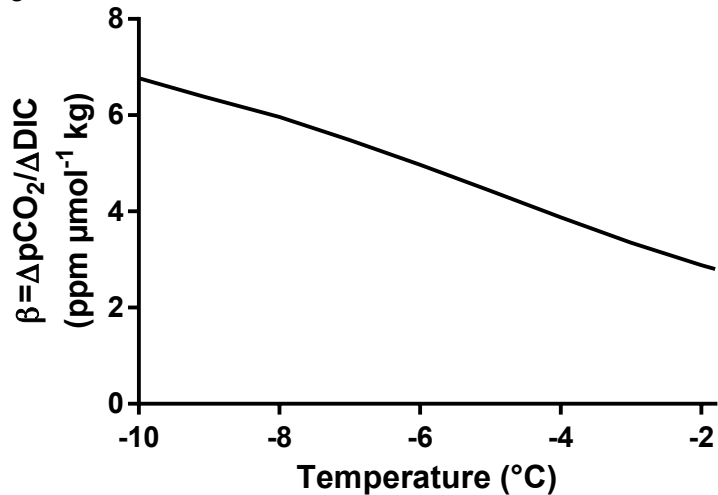


Fig. 9

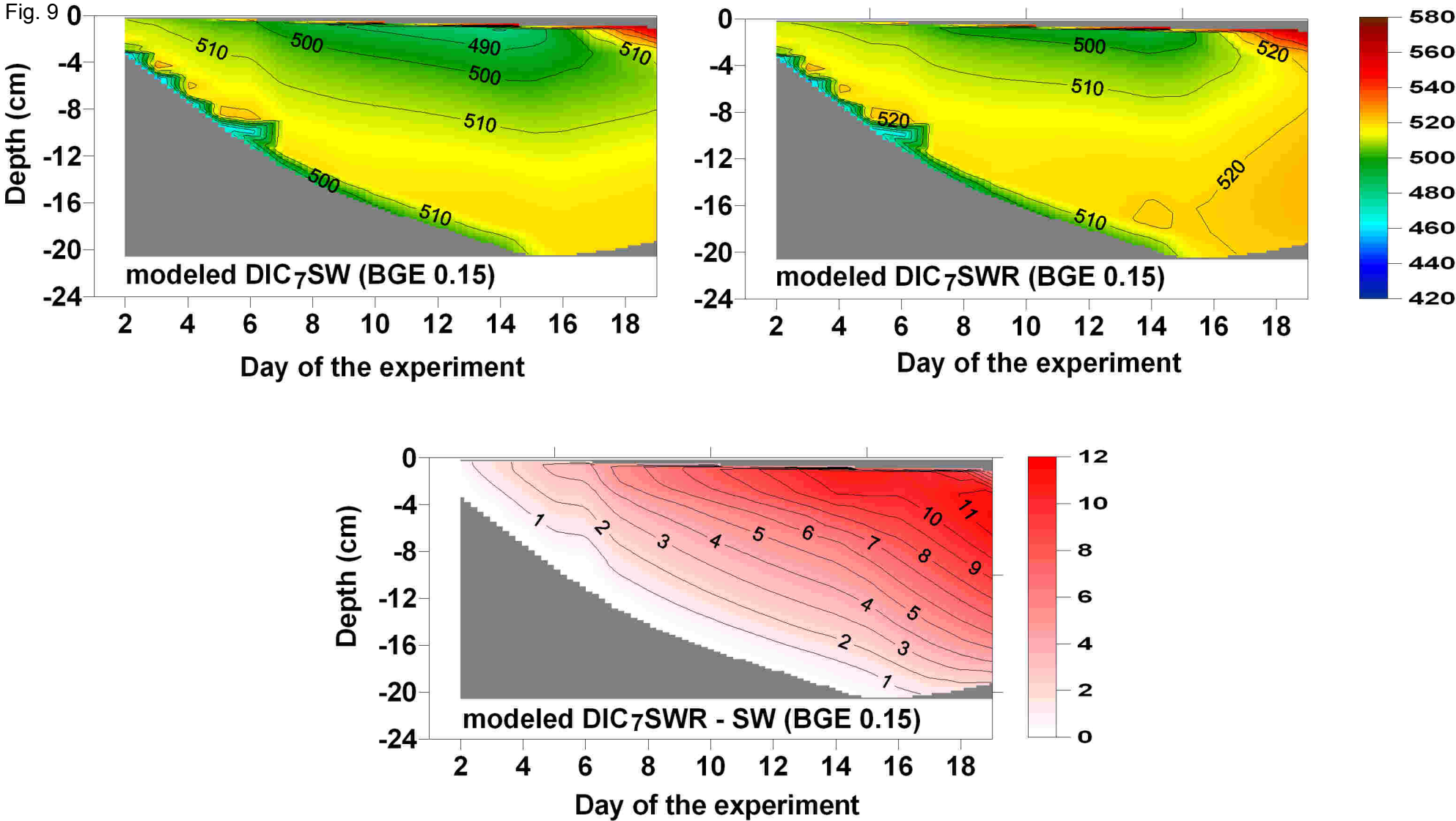


Fig. 10

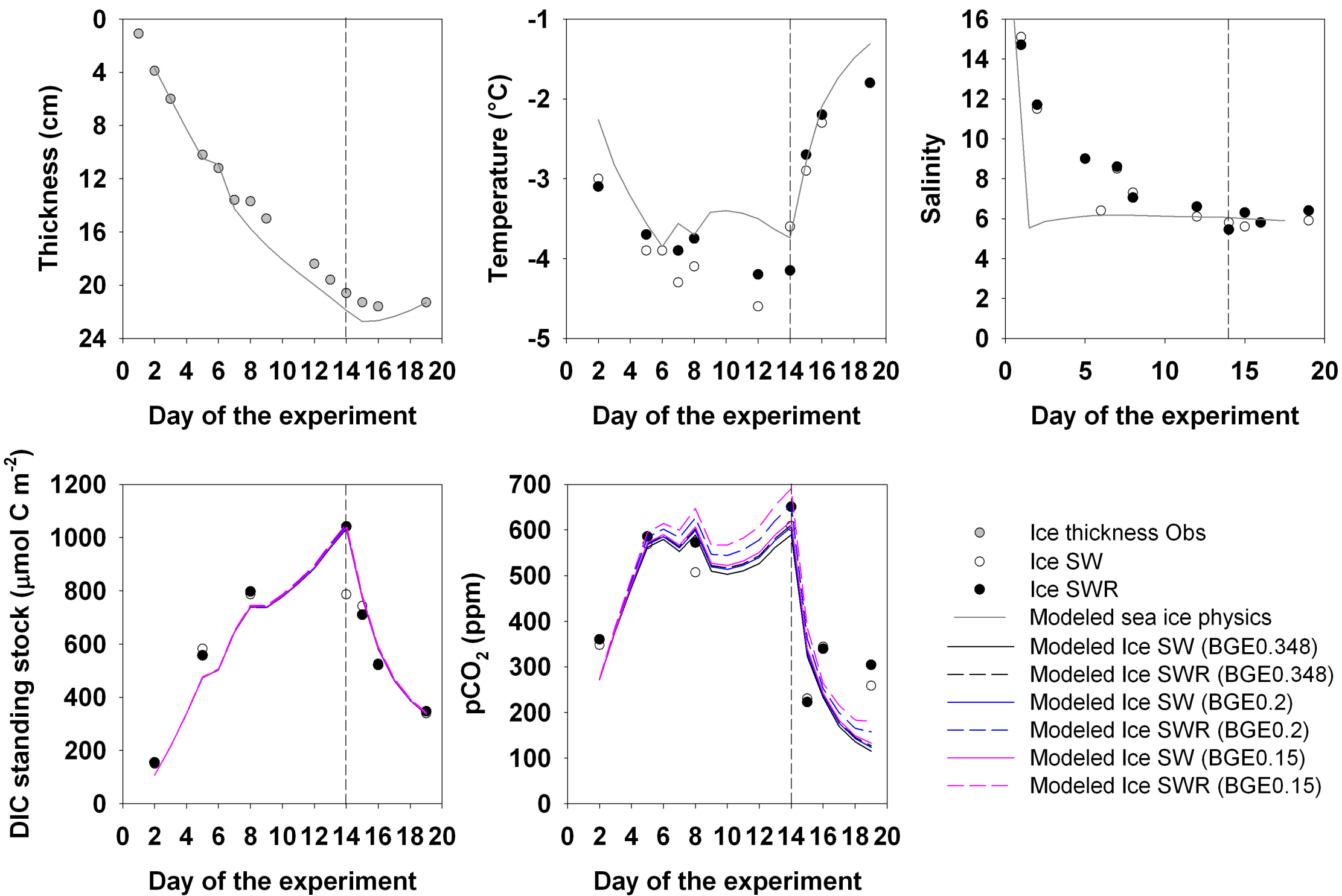


Fig. 110

